Derivation of trophoblast stem cells unveils unrestrained potential of mouse ESCs and epiblast

Debabrata Jana[1], Purnima Sailasree[1], Priya Singh[1], Mansi Srivastava[1,2], Vijay V Vishnu[1], Hanuman T Kale[1], Jyothi Lakshmi[1], Gunda Srinivas[1], Divya Tej Sowpati[1,2*], P Chandra Shekar[1,2*]

[1] CSIR-Centre for Cellular and Molecular Biology; Uppal Road, Hyderabad, Telangana, India 500007.

[2]Academy of Scientific and Innovative Research (AcSIR); Ghaziabad- 201002, India.

*Correspondence: tej@ccmb.res.in; csp@ccmb.res.in

SUMMARY:

mESCs and epiblast are considered to follow strict lineage adherence and lack the potential to contribute to trophoectoderm. Here, we report the derivation of trophoblast stem cells (ESTS) from the mESCs. The single-cell transcriptome and molecular characterization of ESTS show similarity with TSCs. They efficiently integrate into the TE compartment of the blastocyst and contribute to the placenta during development. We discovered GSK3β as a critical regulator of the TE fate of ESCs. It plays a vital stage-specific role during ESTS derivation. We further show β-CATENIN and an intron-I regulatory element of *Cdx2* are essential for the TE fate of ESCs. We further show that the mouse epiblast can readily differentiate into TE lineage. In contrast to the paradigm of the restricted potential of pluripotent ESCs and epiblast, our data shows that murine ESCs and epiblast have the unrestrained developmental potential for extraembryonic lineages.

INTRODUCTION

The mammalian zygote undergoes cleavage followed by the segregation of an outer trophoectoderm (TE) layer and an inner cell mass (ICM) to form the blastocyst. The TE and its cell culture equivalent - trophoblast stem cells (TSCs) can contribute to the extraembryonic tissue -placenta. The ICM further delineates into the epiblast and the primitive endoderm(Cockburn and Rossant, 2010; Gardner and Rossant, 1979). The ESCs derived from the epiblast have restricted potential to contribute to the embryo and primitive endoderm derivatives(Chazaud et al., 2006; Gardner and Rossant, 1979; Plusa et al., 2008). They lack the potential to contribute to the TE derivatives(Gardner, 1983; Nichols and Gardner, 1984) . The textbook model of strict adherence to the restricted lineage potential of the mammalian epiblast and ESCs is being challenged by recent reports of the derivation of TSCs from the human pluripotent stem cells (PSCs)(Dong et al., 2020; Guo et al., 2021; Jang et al., 2022; Wei et al., 2021). However, the ability of such cells to contribute placenta *in vivo* is unverified. Further, the lack of TSCs derived from PSCs of any other mammals continues to support the adherence to the restricted lineage potential of mammalian PSCs. The TSCs induced from the mouse pluripotent stem cells by genetic manipulations involving cellular reprogramming fail to attain the transcriptome and chromatin architecture of the TSC derived from a blastocyst(Cambuli et al., 2014; Kuckenberg et al., 2010; Ng et al., 2008; Nishioka et al., 2009; Niwa et al., 2000; Niwa et al., 2005; Ralston et al., 2010). Despite decades of research efforts, the derivation of TSCs from murine ESCs or epiblast has remained elusive leading to the conclusion of a lack the TE potential(Guo et al., 2021) in murine ESCs and epiblast.

Contrary to the current understanding, we report that the mouse ESCs and the mouse epiblast have the potential to contribute to TE lineage by derivation of TSCs. TSCs can be derived by the priming of ESCs to TE lineage and conversion to TSCs under defined culture conditions. The transcriptome and developmental potential of ESTS are similar to the TSCs. We identified GSKβ activity as the gatekeeper of the TE potential of ESCs. β-CATENIN and *Cdx2*-intron-I regulatory elements are essential for the TE potential of ESCs. We further show that mouse epiblast has the potential readily differentiate into TE lineage cells. We show that mouse ESC and epiblast have full developmental potential to differentiate into all extraembryonic lineages.

64 **RESULTS**

65

66 **Derivation and characterisation of trophoblast stem cells (ESTS) from ESCs**

67 While studying the regulation of core pluripotency factors by GSK3β inhibitor -
68 CHIR99201 (CHIR) and MEK inhibitor PD325901 (PD) in ESC(Ying et al., 2008), we
69 observed cobblestone-shaped cells differentiating around the ESCs in presence of CHIR in
70 serum and LIF (SLCHIR). They morphologically resembled the TE cells differentiated from
71 ZHBTc4 ES cells by doxycycline treatment (ZHBTc4+Dox)(Niwa et al., 2000) (Figure 1A)
72 and expressed TE master regulator *Cdx2*. Other TE factors were induced at some time points
73 of SLCHIR treatment, *Cdx2* transcripts were strongly induced with time in SLCHIR than other
74 TE transcripts (Figure S1A). The expression of *Cdx2* is dependent on the concentration of
75 CHIR, which is reduced by PD in a dose-dependent manner (Figure S1B). The *Cdx2* expression
76 is much higher in SLCHIR than in SL2i. CDX2 protein was expressed in SLCHIR, multiple
77 folds higher than SL2i (PD+CHIR) and ZHBTc4+Dox cells consistent with the transcript
78 levels. GATA3 was detectable in SLCHIR albeit lower than ZHBTc4+Dox cells (Figure 1C,
79 S1C). Immunofluorescence showed only a subpopulation of ESCs expressed CDX2 in
80 SLCHIR and SL2i (Figure 1D). A subpopulation of these cells co-expressed OCT4 and CDX2.
81 Such cells were more frequent in SL2i than in SLCHIR. CDX2 expression was observed in the
82 cells in the periphery of the ESC colony (Figure S1D), where cells mostly primed for
83 differentiation reside. We generated and utilized TCMC-OGFP cell line to understand the
84 origin of these subpopulations. The *Cdx2* expression in TCMC-OGFP is reported by
85 mCherry(Jana et al., 2019) and *Oct4* expression by GFP (Figure S1E). FACS analysis of the
86 SLCHIR treatment time course showed that the OCT4-expressing cells gave rise to *Oct4-Cdx2*
87 double-positive cells. *Cdx2*-mCherry positive cells appear 16hrs onwards (Figure S1F). Most
88 double-positive cells differentiated and lost OCT4 expression when cultured in TS
89 media(Tanaka, 2006). A small proportion of *Cdx2*-expressing cells continued to express *Cdx2*
90 in TS media, which was lost in subsequent passage suggesting that CHIR induced *Cdx2*
91 expression was transient and could not be sustained by self-activation (Figure S1G, H).

92 *Cdx2* overexpression in ES cells represses *Oct4* to induce differentiation to TE and
93 enable derivation of TSCs(Niwa et al., 2005). Transient *Cdx2* induction prompted us to derive
94 TSC from SLCHIR-treated ESC. Our attempts to derive TSCs in TS media(Tanaka, 2006) and
95 defined TSC media for human TSCs(Okae et al., 2018) from ESC treated with or no CHIR
96 failed (Figure 1E, S2A). Although some cells with morphological resembles to TSCs were

97 observed in both TS medias after SLCHIR treatment, they failed to self-renew in subsequent
98 passages. Surprisingly, we could derive and maintain TSC-like cells in FAXY media (bFGF,
99 Activin-A, XAV-939, and Y-27632)(Ohinata and Tsukiyama, 2014) from CHIR-treated ESC
100 (Figure 1E, Figure S2A, B). ESC cultured in SL give rise to TSC-like cells in FAXY at very
101 low frequency, suggesting that priming ESC with CHIR is essential to enhance the efficiency
102 of TSC-like cells derivation (Figure S2A). These results suggest that CHIR partially primes a
103 subpopulation of ESC towards TE lineage by inducing *Cdx2.* We refer to this state of ESC as
104 TSC-primed-ESC. The cells might require further cues to make complete transition to TSCs
105 which are lacking in TS media and human TSC media. However, in FAXY they make complete
106 transition to TE lineage and enable derivation of TSC-like cells from ESC. The TSC-like cells
107 derived from SLCHIR treated ESC were named as ESTS.

108 We supplemented FAXY with CHIR to increase ESTS derivation, surprisingly ESTS
109 could not be derived in FAXY+CHIR (Figure S2C). CHIR promotes β-Catenin signalling
110 while XAV-939(Huang et al., 2009) represses it, suggesting, β-Catenin signalling is essential
111 for the priming stage but inhibitory for the next stage of transition to ESTS. This was further
112 supported by reduced CDX2 and GATA3 expression when a lower concentration of XAV
113 (5nM) was used instead of 10 nM in FAXY (Figure S2D). This data suggest that β-CATENIN
114 has a stage-specific function during the derivation of ESTS. Further, the ESTS established in
115 FAXY could be maintained and cultured for multiple passages in TS media. This suggests that
116 although TS media may support self-renewal of ESTS, TS media may lack the ability to support
117 the initial transition of the TSC-primed-ESC to TE lineage. The ESTS resembled TSCs derived
118 from blastocysts (Figure 1F) and expressed CDX2 and GATA3 (Figure S2D, E). The ESTS
119 could be passaged continuously and can differentiate to TE lineage (Figure 1F). We compared
120 the expression of major TSC markers in ESTS. The expression of *Cdx2, Gata3, Elf5, Tfac2c,*
121 *Eomes,* and *Hand1* in ESTS was comparable to TSCs (Figure 1G).

122 Together our data show that murine ESCs have the potential to contribute to TE lineage.
123 GSK3β activity functions as a gatekeeper of TE lineage and its inhibition primes the ESCs to
124 TE lineage and enable derivation of ESTS in FAXY media.

125

126 **Transcriptome analysis and developmental potential of ESTS**

127 We carried out whole transcriptome analysis of the ESTSs, TSCs and ESCs. In a
128 principal component analysis of the transcriptomes, the ESTSs clustered closer to TSCs
129 suggesting they share similar transcriptome (Figure S3A). Expression of TE markers in ESTS

130 were comparable to TSCs, and the pluripotency transcripts were absent in ESTS (Figure S3B-
131 C). TSC genes like *Elf5, Tfap2c* and *Tead4* known to maintain self-renewal *were* relatively
132 higher in ESTSs than in TSCs, while TSC differentiation gene like *Plet1*, *Krt7*, and
133 *Hand1*(Marchand et al., 2011; Murray et al., 2016) were enriched in TSCs suggesting the self-
134 renewal ability of ESTSs could be similar if not better than the TSCs (Figure S3B).

135 To ascertain the cellular identities, we performed the scRNA-Seq analysis of ESCs,
136 TSCs, and ESTSs. The UMAP revealed an overlap of most ESTS and TSCs in clusters 0,1 and
137 3 in similar proportions. Cluster 2 & 4 represent mostly TSC and ESTS respectively but cluster
138 closely. Together the data suggests that the ESTS are composed of cell types similar to TSCs
139 (Figure 2A-B). Most ESCs are segregated into a distinct cluster 5. The TSCs are characterized
140 by heterogenous culture similar to ESCs. TSC culture is composed of coexistence of multiple
141 developmental transition stages. Most TSC gene like *Sox21*, *Elf5*, *BMP4*, *Sbsn*, *Bmp8b*, *Nat8l*
142 and *Wnt6*(Frias-Aldeguer et al., 2019; Jaber et al., 2022; Li et al., 2013; Ralston et al., 2010;
143 Zita et al., 2015) are enriched in cluster 0 (Figure 2C, S3C). The *Elf5* is repressed by DNA
144 methylation in ESCs, the expression of *Elf5* and other polar TE genes like *Ppp2r2c*, *Eomes*,
145 *Cdx2*, *Ddah1*, *Duox2*, *Cpne3* and *Rhox5*(Frias-Aldeguer et al., 2019) are enriched more in
146 clusters 0, 2 and 4 *(*Figure S3D), suggesting these cluster may represent polar TE
147 subpopulations (Figure S2D). Mural TE markers are distributed across except *Flt1*, *Slc5a5*, and
148 *Slc2a3,* which are enriched partially in other clusters. Together our data suggest that the ESTS
149 have heterogeneity similar to the TSCs and they are composed of large sub-populations of cells
150 with expression of polar TE markers.

151 To exclude the possibility of cross-contamination of TSCs in ESTS culture, we derived
152 ESTS from an ES cell line carrying Ef1a-H2B GFP transgene. ESTS-GFP cells (2 cells) were
153 injected into morula stage embryos to assess their developmental potential. GFP-expressing
154 cells were observed exclusively in the TE layer of the blastocysts. The GFP-expressing cells
155 also expressed TE marker – GATA3 (Figure 2D, S3F). We transferred the blastocysts into the
156 uterus of pseudo-pregnant mice and analysed the contribution of ESTS-GFP cells in E12.5
157 embryos. The ESTS-GFP cells contributed to the placenta, GFP expressing cells were not
158 detected in the embryos (n=46) (Fig.2D-E, S3G). ESTS contributed to the placenta in nearly
159 52% of the chimeric embryos in agreement with contribution reported for TSCs
160 earlier(Cambuli et al., 2014). ESTS-GFP contributed to the labyrinth as well as the junctional
161 zone of the chimeric placenta (Figure 2F, S3H), suggesting ESTS contribute exclusively to TE
162 lineage in developing chimeric embryos. Our data demonstrates that the ESTSs are
163 heterogenous culture with subpopulations sharing transcriptome similar to TSCs. They can

integrate into embryos to form chimeric embryos, participate in devolvement and efficiently contribute to the TE lineage derivatives.

β-CATENIN and Intron-I regulatory region of *Cdx2* are essential for priming of ESC to TSCs

OCT4 and NANOG repress *Cdx2* to inhibit TE lineage(Chen et al., 2009; Niwa et al., 2000). We asked whether *Nanog* or *Oct4* expression levels affect CHIR-induced expression of *Cdx2* and priming of ESCs to TE during ESTS derivation. We utilised *Nanog*:GFP (TNGA)(Chambers et al., 2007) and *Oct4*:GFP (Oct4GiP)(Kale et al., 2022) ESC lines to sort the lowest 10% and highest 10% *Nanog* or *Oct4* expressing cells. The *Cdx2* transcript was analysed after 16hrs of CHIR treatment. *Cdx2* was induced significantly in low-*Nanog* relative to high-*Nanog* population but remained unchanged in *Oct4*-low and high cells, suggesting CHIR induces *Cdx2* in low-*Nanog* cells (Figure 3A). Further, we utilised genetically engineered ESC with different levels of NANOG and OCT4 to analyse the induction of *Cdx2* (Figure 3B). CDX2 was detectable in the presence of CHIR in all the cell lines. Constitutive expression of *Nanog* transgene in the ENOE cell line significantly repressed CDX2. CDX2 was induced multiple folds in *Nanog* null cell line and was barely detectable when NANOG expression was restored from a transgene in TBCR cell line (Figure 3C, S4A) suggesting that NANOG prepresses CHIR mediated induction of CDX2 in a dosage dependent manner. CDX2 was induced in *Oct4*+/- cell in CHIR, surprisingly, it was further increased in cell line with constitutive over-expression of *Oct4*, suggesting that the basal expression levels of OCT4 are essential and sufficient to repress *Cdx2* in ESC (Figure 2C, S4B). However, OCT4 does not show dosage-dependent repression of *Cdx2,* unlike NANOG. To understand how OCT4 and NANOG repress CHIR-induced *Cdx2* expression, we utilised ZHBTc4 cells where *Oct4* could be shut down by Doxycycline to induce differentiation to TE lineage(Niwa et al., 2000). We constitutively over-expressed Flag-Bio-*Nanog* from the transgene in ZHBTc4 to generate ZHBNOE (Figure S4C). Doxy treatment induced expression of CDX2 and GATA3 in ZBHTc4 and ZHBNOE (Figure 3D). Overexpression of NANOG in ZHBNOE failed to repress CDX2 in absence of OCT4 resulting in NANOG-CDX2 positive cells, suggesting OCT4 is essential for repression of *Cdx2* by NANOG (Figure 3D, S4D, S4E). Intriguingly CDX2 is expressed randomly in the *Nanog* null ESC colonies, unlike in WT where CDX2 was mostly restricted to the cells in the periphery of the ESC colony (Figure 3E). We analysed multiple ChIP-Seq data to identify possible regulatory elements for CHIR mediated induction of *Cdx2*. Intron-I region

197 of *Cdx2* was enriched in OCT4, NANOG, TCF3 and β-CATENIN ChIP-seq data.
198 Trophectoderm enhancer (TEE) region upstream of the promotor was enriched in YAP-TAZ
199 ChIP-seq (Figure S4F). We cloned the *Cdx2* promotor (TSS), TEE, and part of intron-I;
200 upstream of a minimal β-Globin promotor driving mCherry reporter (Figure 3F). Reporter cell
201 lines were created by transgenic integration of these constructs in ESC. A significant induction
202 of mCherry was observed in Intron-I reporter cell line after CHIR treatment suggesting CHIR
203 might induce *Cdx2* through intron-I (Figure 3F). Further we deleted the TEE, Intestinal
204 enhancer (IEE), OCT4 binding regions (OBR), NANOG binding regions (NBR) and both
205 (ONBR) in TCMC. CHIR treatment failed to induce *Cdx2*:mCherry in ΔOBR, ΔNBR, and
206 ΔONBR (*Cdx2*-Intron-I) confirming that *Cdx2*-Intron-I is essential for CHIR-mediated
207 induction of *Cdx2* (Figure 3G). Inhibition of GSK3β by CHIR activates β-CATENIN, we asked
208 if β-CATENIN is essential for induction of *Cdx2*. CHIR fails to induce *Cdx2*:mCherry in *β-*
209 *Catenin* null TCMC (Figure S4G). Together our data suggest that CHIR acts through β-
210 CATENIN on Intron-I of *Cdx2* to induce its expression. Both OCT4 and NANOG are together
211 essential for repression for CHIR-induced expression of *Cdx2* and priming of ESC to TSCs.
212

213 **β-CATENIN and Intron-I mediated activation of *Cdx2* is essential for localisation of ESC**
214 **to the TE compartment of blastocyst**

215 The ground state ESCs are cultured in 2iL(Ying et al., 2008), EPSCs (D-EPSCs from
216 Deng laboratory) cultured in LCDM (LIF, CHIR, DiM, MiH)(Yang et al., 2017b), and
217 Expanded PSCs (L-EPSCs from Liu laboratory) in EPSCM (CHIR, LIF, PD0325901,
218 SB203580, A-419259, XAV-939)(Yang et al., 2017a). Intriguingly, apart from LIF, CHIR is
219 the only common small molecule in all these culture conditions enabling enhanced
220 pluripotency. We asked if CHIR-mediated induction of *Cdx2* through β-CATENIN and *Cdx2*-
221 Intron-I is essential for the extraembryonic potential of the ground state ESC and EPSCs.
222 *Cdx2*:mCherry expression was not induced in SLCHIR, 2iL, LCDM, and EPSCM in TCMC
223 cells lacking β-CATENIN (TCMBβ-Cat-/-) implying an essential role for β-CATENIN in
224 *Cdx2* induction (Figure 4A). *Cdx2*:mCherry was induced in TCMC cultured in SLCHIR, 2iL,
225 and LCDM, but not in EPSCM (Figure 4B). Trophoblast factors CDX2 and GATA3 function
226 downstream of TEAD4. Either factor can independently impart trophoblast fate when
227 ectopically expressed in ESCs(Ralston et al., 2010). We asked which trophoblast factors are
228 induced in the above stem cell states to induce trophoblast potential. CDX2 was detected in
229 ESC cultured in SLCHIR, 2iL, and LCDM but not in EPSCM (Figure 4C, S5A). The absence

230 of TEAD4 expression (Figure S5A) suggests that the induction of *Cdx2* in D-EPSCs is
231 independent of TEAD4. We asked if *Cdx2*-intron-I is essential for *Cdx2* expression in these
232 pluripotency states. *Cdx2*:mCherry expression was not induced in 2iL and LCDM in ΔOBR,
233 ΔNBR, and ΔONBR suggesting that the intron-I regulatory regions of *Cdx2* are essential for
234 the activation of *Cdx2* in 2iL (S5B). These data show that β-CATENIN and *Cdx2*-intron-I are
235 essential for *Cdx2* induction in 2iL. However, *Cdx2* expression was not induced in EPSCM
236 despite the presence of CHIR. We reasoned that the presence of XAV in EPSCM could increase
237 stability of AXIN and might inhibit CHIR mediated activation of β-CATENIN and *Cdx2*.
238 Addition of XAV in LCDM significantly reduced the activation of *Cdx2* confirming that XAV
239 counteracts CHIR mediated induction of *Cdx2* (Figure 4B, 4C, S5A). Failure to derive ESTS
240 from TCMBβ-Cat-/- and ΔONBR ESC suggest that the β-CATENIN and *Cdx2*-intron-I are
241 essential for TSC-priming and derivation of ESTS (Figure 4D). Together our data demonstrate
242 that CHIR is the key molecule in 2iL and LCDM that primes TE fate in pluripotent cells by
243 induction of *Cdx2* through β-CATENIN and *Cdx2*-intron-I.

244 We asked if CHIR-induced *Cdx2* could alone enable ESC to contribute to
245 extraembryonic lineage *in vivo*. We injected H2B-GFP-ESC (HGFP) cultured in SL, and
246 SLCHIR into morula (E2.5). The contribution of the injected cells to the three lineages of the
247 blastocysts was analysed by immunostaining at E4.5. The descendant cells of HGFP cultured
248 in SL contributed to the epiblast (Figure 4E). The cells cultured in SLCHIR (TSC-primed-ESC)
249 were mostly localised to the epiblast. They also localised to the TE compartment in 7% of the
250 blastocysts (Figure 4E) suggesting that ESCs cultured in SLCHIR could localize to TE
251 compartment. The cells that localised to epiblast expressed OCT4, However, these cells in the
252 TE compartment neither expressed OCT4 nor CDX2 (Figure 4E). This strengthens our findings
253 that induction of *Cdx2* by CHIR primes the ESC to TE lineage and such priming may be
254 sufficient for their localization to TE compartment. However, the absence of CDX2 expression
255 in derivatives of TSC-primed-ESC suggest that these cells do not acquire bona fide TSC
256 capability. They need additional coaxing cues for the complete transition to TE lineage. Our
257 data is similar to the lack of CDX2 and OCT4 expression in D-EPSCs localised to the TE
258 position as reported by Posfai et. al.(Posfai et al., 2021).

259 We asked if the ability of the ESC in SLCHIR to localise to the TE position in
260 blastocysts is merely due an intermediate stage resulting from induction of *Cdx2* by CHIR or
261 an overall extended potential of the cells. We generated TCMC-ΔONBR ESC carrying an H2B-
262 GFP transgene (ΔONBR-HGFP). The cells were cultured in SLCHIR and injected into morula

263 stage embryos to analyse theirs *in vivo* developmental potential. The injected cells exclusively
264 contributed to the epiblast and failed to localize to TE position, suggesting *Cdx2*-Intron-I is
265 essential for the localisation of these cells to the TE position in the blastocyst (Figure 4E, 4F).
266 Our data suggest that the ability of the TSC-primed-ESCs to localise to TE position in
267 developing blastocyst can be attributed to *Cdx2* induction through Intron-I and may not be due
268 to the overall extended potential of these cells.
269
270 **Derivation of TSCs from mouse epiblast**
271 The ability to develop into the TE lineage is unconstrained in human epiblast but is
272 considered to be lacking in mouse epiblast(Guo et al., 2021). ESTS can be derived from mESC
273 in FAXY, we investigated whether the mouse epiblast had the same potential to differentiate
274 to TE linage. The plasticity of mouse ICM to form trophoblast is lost by mid blastocyst
275 stage(Posfai et al., 2017). We isolated ICM of the mouse embryo after E3.75 by
276 immunosurgery(Solter and Knowles, 1975) and cultured in SL and SLCHIR for 24 hrs. The
277 media was changed to FAXY and cultured for one week (Figure 5A). Outgrowths appeared in
278 both culture conditions. Surprisingly the cells of the outgrowth obtained from
279 SLCHIR→FAXY morphologically resembled endoderm, whereas some of the outgrowths
280 from SL→FAXY resembled TSC morphology (Figure 5B). The outgrowths were picked and
281 cultured further in FAXY. TSC-like cell lines (EpiTS) could be established from the
282 SL→FAXY epiblasts. The EpiTS expressed CDX2 and could self-renew for multiple passages
283 (Figure 5C). The possibility of residual TE cells surviving the immunosurgery giving rise to
284 TSCs cannot be ruled out. To evaluate this possibility, we performed immunosurgery on 96
285 blastocysts. Half of the embryos (48 nos) were randomly chosen for immunostaining with
286 CDX2 and OCT4. The other half (48 nos) were cultured in SL→FAXY condition. Outgrowths
287 from 8 out of 48 (16%) epiblasts could be established into EpiTS. Only one cell in the epiblast
288 of an embryo (2%) was observed to stain for CDX2 after immunosurgery (Figure 5D, 5E)
289 suggesting only 2% of epiblast contained contaminating CDX2 expressing cell. This suggests
290 that the TSC outgrowth appearing after immunosurgery arise mostly from epiblast. To
291 scrutinize this further, we utilized HGFP cells which can contribute only to ICM of the
292 developing blastocyst (Figure 4E) when cultured in SL. We injected HGFP cells cultured in
293 SL into 8 cell embryos and subjected the chimeric blastocyst to immunosurgery and EpiTS
294 derivation (Figure 5F). The immunostaining of the outgrowths from the HGFP chimeric
295 epiblast showed some of the cells co-expressing GFP and CDX2 (Figure 5G) suggesting the

296 epiblast cells were indeed differentiating to TE lineage. The GFP-CDX2 co-expressing cells
297 were found in 20% of the outgrowths (Figure 5G). Collectively, we show that mouse epiblast
298 possesses potential to differentiate to TE linage and EpiTS can be derived from mouse epiblast.
299
300 **Discussion**
301
302 In this study, we have derived TSC from murine ESC by a two-step process. First
303 involving a TSC-priming of ESCs to activate the pioneer transcription factor *Cdx2*(Liang et
304 al., 2021*)* followed by a complete transition to TSC. *Cdx2* transgene expression can convert
305 ESCs to TSCs(Kuckenberg et al., 2010; Niwa et al., 2005). We show that GSK3β inhibition
306 induces *Cdx2* expression in ESCs, however such cells fail to convert to TSC in presence of a
307 GSK3β inhibitor. This could be attributed to pleiotropic effects such as the upregulation of
308 *Stat3* by GSK3β inhibition(Hao et al., 2006), which might interfere in the next stage of
309 complete TSC transition. The essential function of XAV in the second stage of complete TSC
310 transition and failure to derive ES-TSC in the continued presence of CHIR in FAXY supports
311 a stage-specific function for GSK3β in ESTS derivation. Inability of the other TSC media(Okae
312 et al., 2018; Tanaka, 2006) to enable the complete TSC transition underscores the essential
313 stage-specific role of Gsk3β function in ESTS derivation. Expression of *Gata3*, *Tead4*, *Raf*,
314 *Eomes*, and *Tfap2c* can induce TE lineage genes similar to *Cdx2* in ESCs or fibroblasts to
315 generate TSCs(Ng et al., 2008; Nishioka et al., 2009; Niwa et al., 2005; Ralston et al., 2010).
316 We suggest, it might be possible to develop novel culture conditions to derive TSCs from PSCs
317 following a similar approach of TSC-priming of ESCs by small molecule induction of any of
318 these factors or their combinations.
319 The TSC-priming step induces some TE lineage markers including *Cdx2* in ESCs.
320 Although such cells do not acquire bonafide TE lineage potential, they can still localise to the
321 TE compartment in balstocysts. *Cdx2*-intron-I dependent activation of *Cdx2* is essential for
322 TSC-priming and TE compartment localisation of ESCs and EPSCs. We suggest that the rare
323 sporadic contribution of ESCs to the TE compartment in embryos observed by us and
324 others(Beddington and Robertson, 1989; Posfai et al., 2021; Yang et al., 2017b) is a result of
325 the localisation of descendants of TSC-primed pluripotent cells which lack bonafide TE
326 potential.
327 Unlike the human epiblast, mouse epiblast and ESCs are considered to lack the potential
328 to readily contribute to trophoectoderm lineage(Beddington and Robertson, 1989; Gardner,

329 1983; Guo et al., 2021; Nichols and Gardner, 1984; Posfai et al., 2017). The chromatin-based
330 lineage barriers were speculated to restrict the Trophoectoderm potential of the mouse epiblast
331 and ESCs(Boyer et al., 2006; Ng et al., 2008; Zijlmans et al., 2022). Recently the histone
332 posttranslational modifications (hPTMS) were found to be largely persevered between hPSC
333 and mESCs suggesting, chromatin barriers may not be major mechanism by which the mouse
334 epiblast/mESC potential is restricted(Zijlmans et al., 2022). Failure to derive TSC from mouse
335 ESC by us and others using the methods used for human TSC and derivation of ESTS in FAXY
336 reaffirms this proposition.

337 The extra embryonic lineages subserve the development of the epiblast to ensure
338 successful development of the progeny and perpetuation of the species. The segregation of
339 epiblast and extraembryonic layers are essential for proper compartmentalization and
340 development. Any damage to the extraembryonic layer cells can affect the development of the
341 epiblast. Hence, we propose that the mammalian epiblast has inherent plasticity to differentiate
342 to extraembryonic layers well beyond the timelines of these linage segregations during
343 development. This inherent potential is restricted by multiple developmental signals and the
344 organization of the embryonic layers. In instances of damage to the extra embryonic layers the
345 epiblast cells can differentiate to the cells of TE or PE compartment to compensate for the lost
346 cells and ensure continued development of the epiblast. The lineage restriction imposed by the
347 developmental signals on the epiblast may be overcome by the signals generated by the damage
348 to the extraembryonic layers. This is best exemplified from our immunosurgery experiments
349 and by Guo et. al., where the damage to TE leads to differentiation of TE from mouse and
350 human epiblast and further supported by development of reformed blastocoel from the ICM of
351 bovine with a TE layer. The development of blastoids entirely from PSCs of human(Kagawa
352 et al., 2022), monkey(Li et al., 2023) and mice(Jana et al., 2023) supports the existence of
353 inherent plasticity in mammalian epiblast and PSCs to generate all extraembryonic lineages.

354 Collectively, our data demonstrate that the mouse ESCs have unrestricted
355 developmental potential contrary to the prevailing understanding. Under appropriate
356 conditions, the unrestrained potential of mESC can be unlocked to derive TSCs. The
357 demonstration of the unrestrained developmental potential of murine and human PSCs opens
358 up the possibility to harness the extraembryonic and blastoid generation potential in other
359 mammalian PSCs by developing appropriate culture approaches.

360 We suggest that there are multiple layers of lineage barriers -like signaling barriers
361 (mechanical and cytokine), Pluripotency factors, chromatin-based barriers operating in
362 different mammalian species which need to be overcome for realization of the full

363 developmental potential of the epiblast. We speculate that a typical mammalian epiblast is not
364 governed by strict adherence to restricted lineage but by an adaptive lineage potential which
365 restrict TE line under normal development, but can permit differentiation to TE linage when
366 the need arises.

367

368 **Acknowledgments:**

369 D.J, V.V.V, M.S was supported by a fellowship from UGC (India). H.T.K was supported by a
370 fellowship from ICMR (India). We thank the Microscopy, FACS, Animal House and
371 transgenic core facilities of CCMB for the support extended to carry out this work. P.Si
372 acknowledges the stipend support from the DBT grant GAP0546. WT/DBT India Alliance
373 grant 500053/Z/09/Z -P.C.S., Department of Biotechnology grant
374 BT/PR14064/GET/119/16/2015-P.C.S., DBT grant GAP0582:
375 BT/PR40264/BTIS/137/44/2022 -D.T.S.

376

377 **Author contributions:**

378 Conceptualization, D.J, and P.C.S Methodology, D.J, P.Si, P.Sa, J.L, G.S, and P.C.S;
379 Investigation, D.J, P.Si, P.Sa, and D.T.S; Writing – Original Draft, D.J, P.Si and P.C.S.;
380 Writing – Review & Editing, D.J, P.Si, D.T.S and P.C.S.; Funding Acquisition, D.T.S and
381 P.C.S.; Resources, D.J, M.S, V.V.V, and H.T.K; Visualization, P.Si and D.J.; Supervision,
382 P.C.S.

383

384 **Figures**

385

386 **Fig. 1. Derivation and characterization of ESTS from mouse ESC**. A) Phase contrast
387 images of E14Tg2a cultured in SL, SLPD, SLCHIR, SL2i, and ZHBTc4 cells cultured in the
388 presence and absence of doxycycline (scale bar=100µm). TE-like cells in SLCHIR are marked
389 with the yellow arrow. B) Quantitative expression analysis of TE lineage genes in indicated
390 culture conditions, error bar represents SD of the mean of biological replicates (n=3). '*'
391 indicates a p-value <0.05, '**' indicates a p-value <0.01, 'ns' indicates a p-value > 0.05. C).
392 Immunoblot analysis of GATA3, CDX2, and OCT4 in indicated culture conditions of E14Tg2a
393 and ZHBTc4 cells. D) Immunofluorescence analysis of CDX2 and OCT4 in E14Tg2a and
394 TSCs derived from the blastocyst. Scale bar = 50µm. E) The experimental scheme depicting
395 the derivation of ESTS from mouse ESCs. F) (Left) Phase contrast images of TSCs derived

396 from the blastocyst and ES-TSCs derived from ESCs. Scale bar = 100µm. (Right) Relative
397 mRNA abundance of TE differentiation genes analyzed by q-RTPCR in 0, 2nd, 4th, and 6th day
398 of differentiation. G) Relative mRNA abundance of TE and pluripotency genes analyzed by q-
399 RTPCR. The error bar represents the SD of the mean of biological replicates (n=3). '*' indicates
400 a p-value <0.05, '**' indicates a p-value <0.01, '***' indicates a p-value <0.001, 'ns' indicates
401 a p-value > 0.05.
402
403 **Fig. 2. Single-cell transcriptomics of ESTS and its characterization** A) UMAP projection
404 of ESC, TSC, and ESTS from sc-RNA Seq analysis. B) Cluster analysis of the UMAP
405 projection of ESC, TSC, and ESTS from sc-RNA Seq analysis. C) Heatmap of the top 50 genes
406 differentially expressed in different clusters of ESC, TSC, and ESTS from sc-RNA seq. D)
407 (Top) Schematic showing injection of GFP labelled ESTS (ESTS-GFP) into 8-cell stage
408 embryo and contribution of ESTS in blastocyst and placenta. (Left bottom) Representative
409 image showing the contribution of GFP labelled ESTS in the TE layer of the blastocyst (marked
410 with yellow arrow). (Right bottom) Representative image showing the contribution of GFP
411 labelled ESTS descendant cells to the placenta at E12.5 (Fluorescence channel was acquired in
412 tile scan). Scale bar =10mm. E) Summary of the contribution of GFP labelled ESTS to the
413 placenta at E12.5. F) Immunofluorescence assay for detection of GFP-positive ESTS in the
414 placental section. DC, JZ and LB depict the decidual region, junctional zone, and labyrinth
415 region of the placenta respectively. Scale bar = 2000µm.

416 **Fig. 3. β-CATENIN and Intron-I regulatory region of Cdx2 are essential for priming of**
417 **ESCs to TSCs.** (Left) FACS profiles of TNGA and Oct4Gip cell line. The 10% low and 10%
418 high GFP expressing cells were sorted, plated, and treated differentially with CHIR for 16 hours
419 (Right) q-RTPCR analysis of Cdx2 expression relative to E14Tg2a in the 10% low and 10%
420 high GFP expressing cells (n=3) '*' indicates a p-value <0.05, '**' indicates a p-value <0.01.
421 B) List of cell lines describing the genetic manipulation of Oct4 and Nanog. C) (Left)
422 Immunoblot analysis of CDX2 and NANOG in the indicated ESC lines cultured in SL and
423 SLCHIR. (Right) Immunoblot analysis of CDX2 and OCT4 in the indicated ESC lines cultured
424 in SL and SLCHIR. D) Immunoblot analysis of NANOG, OCT4, CDX2, GATA3, and β-
425 ACTIN in ZHBTc4 (ZHB) and ZHBTc4 NOE (expressing a Nanog transgene). E) (Left)
426 Immunofluorescence detection of CDX2 and OCT4 in CHIR-treated WT and Nanog null cell
427 line. (Scale bar = 100µm). (Right) Distribution of fluorescence intensity of CDX2 and OCT4
428 across a colony. F) (Top) Schematic depicting the DNA constructs used for the mCherry

429 reporter assay to assess the Cdx2 regulatory elements in ESCs. (Bottom) histogram profile of
430 mCherry expression observed in stable ESC lines carrying Cdx2 regulatory elements reporter
431 treated with or without CHIR. G) Contour plots showing the expression of mCherry in TCMC,
432 TCMCΔTEE, TCMCΔOBR, TCMCNBR, TCMCΔONBR, and TCMCΔIEE treated
433 with/without CHIR.

434 **Fig. 4. β-CATENIN and Intron-I mediated activation of Cdx2 is essential for localisation**
435 **of ESCs and EPSCs to the TE compartment of the blastocyst** (A) mCherry expression in
436 TCMCβ-Cat-/- cell line cultured in SL, SLCHIR, 2iL, LCDM, and EPSCM. (B) (Top left)
437 mCherry expression in TCMC cell line cultured in SL, SLCHIR, LCDM, and EPSCM (top
438 right) Relative quantification of mean fluorescence intensity of mCherry (n=3). (Bottom left)
439 mCherry expression in TCMC cell line cultured in LCDM and LCDM+XAV. (Bottom right)
440 relative quantification of mean fluorescence intensity of mCherry (n=3), '***' indicates a p-
441 value <0.001. (C) (Top) immunoblot analysis of CDX2 and β-ACTIN in E14Tg2a and TSC in
442 indicated culture conditions. (Bottom) relative CDX2 levels as estimated by densitometry
443 (n=3) '*' indicates a p-value <0.05, '**' indicates a p-value <0.01. (D) Schematic
444 representation of method followed to derive ESTS from TCMCβ-Cat-/- and TCMCΔONBR
445 cell lines. (E) (Left) Immunostaining of CDX2 and OCT4 in chimeric blastocysts developed
446 from morula injected with HGFP and DONBR-HGFP ESCs cultured in SLCHIR or LCDM.
447 (Scale bar =50µm). (Right) Table summarizing the outcomes of the chimeric blastocyst
448 experiments. (F) Schematic representation of experiment to evaluate the chimeric potential of
449 HGFP and DONBR- HGFP cell lines cultured in SLCHIR or LCDM.

450 **Fig. 5. Derivation of TSCs from mouse epiblast.** A) Schematic of the derivation of TS-like
451 cells from E3.75 mouse blastocyst (EpiTS). B) Phase contrast image of TS-like outgrowth
452 cultured from post-immunosurgery blastocyst under depicted culture conditions. C)
453 Immunostaining of CDX2 in EpiTS derived from ICM. Scale bar = 50µm. D) Immunostaining
454 of CDX2 and OCT4 in embryos following immunosurgery treatment. (Top row)
455 Immunostaining E3.5 blastocyst (Middle and bottom row) Immunostaining of E3.5 embryo
456 post immunosurgery. The yellow marked arrow marks the single CDX2 positive cell in an
457 embryo out of 48 embryos analysed. Scale bar = 50µm. E) Table summarizing the number of
458 embryos having CDX2 expressing cells and number of TS-like outgrowth after
459 immunosurgery. F) (Top) Schematic showing injection of GFP labelled ESCs (HGFP) into 8-
460 cell stage embryo followed by EpiTS derivation from the chimeric blastocyst. (Left Bottom)
461 Phase contrast image overlaid in GFP channel showing the contribution of HGFP in E3.5

462 blastocyst. (Right Bottom) The Phase contrast image overlaid in the GFP channel shows the
463 contribution of the HGFP Epi-TS colony. Scale bar = 50µm. G) (Top) Immunostaining of
464 CDX2 and GFP in EpiTS colony. (Bottom) Table summarizing the number of HGFP-injected
465 embryos and the number of TS-like outgrowth coexpressing GFP and CDX2. Scale bar =
466 50µm.

467 **Methods**

468 **Culture of metastable and ground-state mouse ES cells**

469 Metastable ES cells were grown on 0.1% (w/v) gelatin-coated cell culture dishes in serum+
470 LIF media, comprising 10% (v/v) heat-inactivated FBS in GMEM (12.5g/litre w/v), NaHCO3
471 (32.7mM), Sodium Pyruvate (1mM), NEAA (0.1mM) and β-mercaptoethanol (0.1mM) and
472 LIF. Ground state ES cells were cultured on 0.1% gelatine-coated tissue culture-treated dishes
473 in N2B27, containing DMEM/F12 and Neurobasal medium in 1:1 (v/v) ratio, supplemented
474 with N2 supplement (1X), B27 supplement (1X), NaHCO3 (32.7mM), Sodium Pyruvate
475 (1mM), NEAA (0.1mM), and β- mercaptoethanol (0.1mM) along with recombinant hLIF
476 (1000U/ml), CHIR99021 (3µM) and PD0325901 (1µM). TrypLE-EDTA was used for
477 dissociation and passing once the confluence reached 70%.

478 **Extended pluripotent stem cell culture**

479 Metastable ES cells were converted into Extended pluripotent stem cells (EPSCs) when grown
480 in either of two different culture regimes. First as described by Pentao Liu's group(Yang et al.,
481 2017b), where DMEM/F12 (Invitrogen), 20% (v/v) KnockOut Serum Replacement (KSR),
482 NEAA (1X), β- mercaptoethanol (0.1mM) and hLIF 1000 U/ml supplemented with the
483 following small-molecule inhibitors: CHIR99021 (3µM), PD0325901 (1µM), JNK Inhibitor
484 VIII (4µM), SB203580 (10µM), A-419259 (0.3µM) and XAV939 (5µM). The second culture
485 media as described by Hongkui Deng's group(Yang et al., 2017b) where basal N2B27 media
486 was supplemented with small molecules and cytokines as follows: 10 ng/ml recombinant hLIF,
487 CHIR99021 (3µM), (S)-(+)-Dimethindenemaleate (2µM), Minocycline hydrochloride (2µM)
488 and 5mg/ml BSA. Upon 70% confluency, EPSCs were passaged with TrypE-EDTA, and
489 splitting was done in a 1:3 ratio.

490 **Derivation of ESTS from ES cells and TSC from blastocyst**

491 For the derivation of trophoblast stem cells (ESTS) from mESCs, E14Tg2a cells were cultured
492 for 48hrs in SL media supplemented with CHIR99021 (3µM). Thereafter, cells were passaged

493 and seeded onto culture plates as described by Ohinata et. al.(Ohinata and Tsukiyama, 2014).
494 Geltrex (1x) or 15µg/ml fibronectin solution in PBS was used to coat the tissue culture-treated
495 plates at 37oC for 1 hour. SLCHIR-treated E14Tg2a cells were seeded onto these plates and
496 cultured in CDM/FAXY media. CDM/FAXY media contained DMEM/F12: Neurobasal media
497 (1:1 v/v), supplemented with N2 (1X) and B27 (1X) supplements, BSA (0.05% v/v), 1-
498 thioglycerol (1.5 X 10-4M), recombinant human bFGF (25ng/ml), recombinant human Activin
499 A (20 ng/ml), XAV939 (10 nM), and Y27632 (5nM). By day 6, colonies with TS-like
500 morphology were surrounded by contaminating non-TS-like cells. Two methods were used to
501 separate ESTS from the contaminating cells. First, by manually picking the colonies having
502 TS-like morphology with a fine pipette and seeding them back into coated dish with FAXY
503 media as a single cell suspension. In another method, CDM/FAXY media was removed, and
504 the culture was treated with Accutase for 30sec or until the contaminating cells started to detach
505 from the dish after gentle tapping. The dishes were washed with PBS to remove the detached
506 cells, while the TS-like cells remained attached. This method utilises the deferential sensitivity
507 of the TS-like cells and the contaminating cells to the Accutase treatment. Media was changed
508 every 24hrs and clearing of contaminating cells was done after the cell density reached 60%
509 confluency. The first cleaned ES-TSC plate was named ESTSP1 followed by multiple passages
510 as P2-P24. ESTSP24 or later passages are hereinafter called ESTS. TSC were derived from
511 blastocysts as described in Ohinata et. al.(Ohinata and Tsukiyama, 2014).

512 **Mice**

513 CD1 and F1 (C57BL6/CBA) mice were obtained from Jackson laboratories. Animal model
514 experiments were carried out following the Institutional Animal Ethics Committee (IAEC) of
515 the CCMB's ethical standards and received approval from the Committee for Control and
516 Supervision of Research on Animals (CPCSEA). For pseudo-pregnancy, Vasectomized F1
517 male mice were mated with CD1 female mice that were 8 to 11 weeks old and in the estrus
518 cycle. All the experimental mice were kept in a 12-hour light/12-hour dark cycle with free
519 access to food and water in a facility with controlled temperatures (18-22ºC) and humidity
520 (R.H. 40-70%).

521 **Superovulation of mice**

522 5 IU of PMSG (pregnant mares' serum gonadotrophin) was administered to female F1
523 (C57BL6/CBA) for superovulation. 5 IU of human chorionic gonadotrophin (HCG) was
524 administered 48 hours after the initial injection and Day 0 was designated of and the subsequent

525 instant mating with F1 male mice. After the vaginal plug was found the following day, 0.5 dpc
526 zygotes were retrieved and cultivated in KSOM in an incubator that was humidified and
527 maintained at 37ºC.

528 **Culture of mouse embryos**

529 The upper portion of the oviduct (ampulla) was cut-off from the pregnant mice, and zygotes
530 (0.5dpc) and cumulus mass were extracted from F1 (C57BL/6J X CBA). A prepared M2
531 medium with 0.3 mg/ml hyaluronidase was used to transfer the oviduct area containing the
532 zygotes. Close to the location of the zygotes, the ampulla was torn using a 26-gauge needle.
533 For a short period of time, all of the zygotes were incubated in M2 medium containing
534 hyaluronidase. Zygotes were picked up using a pipette after the cumulus mass had fallen off
535 and transferred to new M2 drops before being recorded as Day 1 and pre-equilibrated at 37ºC
536 with 5% CO_2 in a humid incubator. Every 24 hours, embryos were transferred into fresh KSOM
537 drops.

538 **Immunosurgery of E3.5 blastocyst**

539 The immunosurgery technique was used to separate the inner cell mass (ICM) and
540 trophectoderm (TE) of mice E3.5 blastocyst(Solter and Knowles, 1975). The blastocysts were
541 transferred to the M2 medium and washed twice in the M2 medium. Blastocysts were incubated
542 with Rabbit anti-mouse antibody at a dilution of 1:10 (diluted in DMEM plus 10% FBS) for
543 15 minutes at 37°C in a CO2 incubator. Blastocysts were washed three times with M2 medium
544 after the incubation. Blastocysts were transferred to a fresh drop containing native guinea pig
545 serum complement at a dilution of 1:50 (diluted in DMEM plus 10% FBS), and incubated for
546 30 minutes at 37°C in a CO2 incubator. The blastocysts were then observed under a microscope
547 to confirm the lysis of the TE cells. Zona pellucida was cleared with acid Tyrode treatment for
548 2 mins. The ICMs were collected carefully using a micropipette and transferred to a new dish
549 with fresh M2 medium. Finally, the ICMs recovered were transferred to Geltrex coated cell
550 culture plate containing FAXY media for EpiTS differentiation.

551 **Injection of ESCs, CHIR-treated ESCs, and ESTS into an 8-cell embryo**

552 GFP expressing ES (HGFP) (cell line pedigree chart in supplementary data) cells were cultured
553 on SL, SLCHIR (CHIR, 3μM) for 16hrs. SLCHIR media was changed freshly 3hrs before
554 injection. For ESTS transfer, GFP labelled ESTS cells which were grown in FAXY for 24
555 passages (ESTSP24) or later passages cells were trypsinized with TrypLE-EDTA, neutralized,

556 washed, and resuspended as single cells in injection media. Injection media was freshly made
557 and constituted of DMEM/F12 (Sigma) supplemented with 10% (v/v) heat-inactivated ES
558 qualified serum, Glutamax (1X), NaHCO3 (32.7mM), and pH was adjusted to 7.2.
559 Resuspended ESCs were microinjected into the 8-cell stage embryo in an injection drop
560 containing 200µl of injection media in a 50mm glass-bottom dish. Leica DM IRB inverted
561 microscope was used with an Eppendorf TransferMan NK2 micromanipulator. The outside and
562 inside diameters of the holding pipette were 95–105µm and 20–25µm respectively; whereas
563 the outside and inside diameters of the injection pipette were 18–20µm and 16–18µm
564 respectively. 2-3 ESCs/ESTS cells were microinjected per embryo on a 50mm dish containing
565 injection media on a microscopic stage maintained at 100C. A batch of 20 embryos was injected
566 in an hour.

567 **Cryosectioning of placental tissue and cytohistochemistry**

568 Placental tissues were obtained after dissecting 12.5 dpc mice. Tissues were immediately fixed
569 in 4% paraformaldehyde and kept overnight at 4ºC. Tissues were washed thrice with PBS and
570 transferred to 15% sucrose solution in PBS and kept at 4ºC until the tissues were sunk at the
571 bottom of the tube. The tissues were again transferred to 30% sucrose solution in PBS and kept
572 at 4ºC overnight followed by OCT media embedding and taken for cryosectioning. Sections of
573 15-micron thickness were taken on ProbeOn slides and followed for immunocytochemistry.
574 The slides were dried at room temperature for 5mins and washed with PBS twice to remove
575 the OCT. Sections were blocked and permeabilized in a blocking buffer containing PBS with
576 5% (w/v) BSA, and 0.3% (v/v) Triton-X 100 for 60 minutes at room temperature. Primary
577 Antibodies were diluted in antibody dilution buffer (ADB) containing PBS with 1% (w/v)
578 BSA, and 0.3% (v/v) Triton-X 100. Sections were incubated with primary antibodies for 4ºC
579 overnight. Sections were washed 3 times with PBS and incubated with secondary antibodies
580 diluted at 1:1000 in ADB. Sections were washed with PBS and mounted with Vectashield (H-
581 1200) containing DAPI.

582 **Generation of CRISPR-based gene knock-out cell lines**

583 The twin guide strategy was used for generating knock-out in ES cells as described in Kale et.
584 al.(Kale et al., 2022). The cell line was characterized by genotyping, qPCR, and western
585 blotting analysis to confirm the intended genetic manipulation. The detailed characterization
586 and pedigree of the cell lines used in this study are provided in supplementary data
587 (supplementary appendix).

588 **Generation of ES cells knock-in cell lines**

589 TCMC cell line was generated by using CRISPR as described by Jana et al. (Jana, et al. 2019).
590 TCMC-OGFP cell line was generated by nucleofecting 1µg supercoiled Oct4-IRES-eGFP-
591 PGK-Neo (Addgene #48681) plasmid to 1 million TCMC using P3 primary cell 4D-
592 Nucelofector X kit (Lonza). Nucleofected cells were plated and grown in SL media
593 supplemented with G418 for 10 days. A single colony was picked up and cultured as replicas
594 in 96 well format for genotyping. The detailed characterization and pedigree of the cell lines
595 used in this study are provided in supplementary data (supplementary appendix).

596 **Immunofluorescence staining**

597 Cells were cultured in 2D culture in 24 wells for up to 70% confluency. Cells were washed
598 thrice with 500µl of PBS and 500 µl of freshly prepared 4% paraformaldehyde (made in PBS)
599 fixative was added to the plate and incubated at RT for 20 minutes. The fixative was removed
600 and the plate was washed thrice with 1ml PBS. The specimen was blocked and permeabilized
601 in a blocking buffer containing PBS with 5% (w/v) BSA, and 0.3% (v/v) Triton-X 100 for 60
602 minutes at room temperature. Primary Antibodies were diluted in antibody dilution buffer
603 (ADB) containing PBS with 1% (w/v) BSA, and 0.3% (v/v) Triton-X100. Specimens were
604 incubated with primary antibodies for 4ºC overnight. Cells were washed 3 times with PBS and
605 incubated with secondary antibodies diluted at 1:1000 in ADB. Cells were washed with PBS
606 and mounted with Vectashield (H-1200) containing DAPI.

607 For staining 3D structures like embryos, they were first washed twice with PBS. Structures
608 were fixed in 4% paraformaldehyde in PBS for 15 minutes and rinsed in PBS containing 3
609 mg/ml polyvinylpyrrolidone (PBS/PVP). Thereafter structures were permeabilised in
610 PBS/PVP containing 0.25% Triton X-100 for 30 minutes. Blocked in blocking buffer,
611 comprising PBS containing 5% BSA, 0.01% Tween 20 for 60 minutes. Primary antibodies were
612 diluted with the appropriate antibody dilution as per the manufacturer protocol in PBS
613 containing 1% BSA, and 0.01% Tween 20 and incubated at 4°C overnight. They were rinsed
614 three times in blocking buffer for 5 minutes each and incubated with secondary antibodies
615 diluted as 1:500 in PBS containing 1% BSA, 0.01% Tween 20, and incubated for 60 minutes
616 at room temperature. Rinsed 3 times with PBS and stained for nuclei with DAPI (1µg/ml)
617 prepared in PBS for 15 minutes at RT. Embryos were finally rinsed 3 times in PBS and images
618 were acquired by confocal microscopy.

619 **Real-time PCR analysis**

620 The RNA was extracted from 1 million cells with TRIzol by manual method and quantified by
621 Nanodrop (Thermo Scientific). One microgram of RNA was reversed and transcribed into
622 cDNA by using SuperScript™ III First-Strand Synthesis System. The first strand synthesized
623 cDNA was diluted 5 times and real-time PCR was set with power SYBR Green PCR master
624 mix on the ABI 7900 HT. The PCR setup was as follows: Step 1: 95ºC for 10 min, step 2: 95ºC
625 for 15 sec, step 3: 60ºC for 30 sec, and Step 4: 72ºC for 30-sec Steps 2-4 were repeated for 40
626 cycles. GAPDH was used as an internal control. The reactions were analyzed by the software
627 (SDS 2.1) provided with the instrument. The primers used for real-time PCR are given in the
628 resource table.

629 **Western blot analysis**

630 The cells were harvested by scraping them from the plates in PBS and collected by
631 centrifugation. The cell pellet was washed twice with PBS and reconstituted in RIPA. RIPA
632 buffer constituting 25mM Tris HCl (pH 8.0), 150mM NaCl, 1% NP-40, 0.5% Sodium
633 deoxycholate, 0.1% SDS, and Complete Protease Inhibitor Cocktail Tablets (Roche). The
634 lysate was sonicated in Bioruptor (Diagenode) and centrifuged. The clear supernatant was
635 transferred to the fresh tube. The protein samples were denatured in loading dye containing β-
636 mercaptoethanol and resolved by SDS-PAGE. Resolved samples were then transferred onto a
637 polyvinylidene difluoride (PVDF) membrane and blocked-in blocking buffer containing 5%
638 non-fat milk in TBST. Primary antibody hybridisation was carried out overnight at 4ºC in 3%
639 non-fat milk in TBST. After incubation three washes were performed with TBST. The
640 secondary antibody was diluted at 1:10,000 in 3% non-fat milk in TBST and incubated for an
641 hour at RT. After incubation three washes were performed with TBST and visualized using
642 enhanced chemiluminescence (ECL) detection kit (Thermo Scientific) and developed in Chemi
643 doc MP (Biorad).

644 **FACS analysis**

645 70% confluent culture was made into single-cell suspension using TrypLE for 4 mins at 37ºC.
646 The cells were diluted in media and pelleted by spinning at 300g for 5 mins. The media was
647 removed and around 1 million cells were resuspended in 300 µl of PBS containing 2% FBS.
648 The cell samples were directly taken for analysis either in Gallios (Beckman Coulter B5-R1-
649 V2) FACS analyzer or LSR Fortessa (BD) analyzer and data was recorded. The FACS data
650 were analyzed using FlowJo vX.0.7

651 **Bulk RNA-seq library preparation**

652 Using the TRIzol reagent and the manufacturer's instructions, total RNA was extracted from
653 ESCs, TSCs and ESTSCs. A total RNA of 1µg was used to generate libraries using of Illumina
654 stranded total RNA prep with Ribo-Zero Plus library preparation kit (Illumina, 20040529). The
655 Qubit dsDNA HS (High Sensitivity) Assay Kit (Invitrogen, Q32854) was used to measure
656 library concentration, and different libraries were combined to create the final pool at an
657 equimolar ratio. Using an Illumina NovaSeq 6000 instrument, libraries were sequenced for a
658 read length of 151 bp reads and a read depth of approximately 30 million reads.

659 **Bulk RNA-seq data analysis**

660 Paired-end Bulk RNA sequencing was done for ESCs, TSCs and ESTSCs. The quality
661 assessment of raw data was done by FastQC v0.11.9 and Illumina universal adapter content
662 was removed using cutadapt v2.8. The filtered sequencing reads were mapped to the mouse
663 reference genome mm10 and Gene counts were obtained by STAR_2.5.4b. The data showed
664 an average of 81% uniquely mapped reads which were annotated with the Ensembl database.
665 Transcripts Per Kilobase Million (TPKM) were calculated by the rsem-calculate-expression
666 function of RSEM v1.3.3. DESeq2 v1.30.1 was used to get the differentially expressed genes
667 based on the Bayes theorem. Genes showing expression of at least 50 in a row were retained
668 for further analysis. Principal component analysis (PCA) and heatmap analysis were performed
669 with the functions plotPCA and pheatmap in R. The visualization of differential expression of
670 marker genes was performed on TPM counts after scaling and normalizing the read counts by
671 row.

672 **Single RNA-seq library preparation**

673 Single-cell suspension was made from ESCs, TSCs and ESTSCs using the TrypLE-EDTA
674 solution. Live cells were sorted as PI-negative populations using a FACS sorter. Approximately
675 5000 cells were loaded for Library preparation using Chromium Next GEM Single Cell 3'
676 Reagent Kits v3.1 (10x genomics). Libraries were sequenced for a read length of 91 bp reads.

677 **Single-cell RNA-seq data processing**

678 Single-cell RNA-sequencing was performed using the 10X Genomics Chromium system and
679 Illumina base call files (BCL) were demultiplexed using the mkfastq function of cellranger
680 v6.0.2 which is specific to 10X libraries. Reads were aligned against mouse reference mm10
681 and filtered by the count pipeline to get the feature, barcode, and gene matrices. The R package
682 Seurat v4.0.1 was used to analyze the feature-barcode matrix. The quality assessment of data

683 was done by scater v1.18.6. Scrublet, a python tool, was used to calculate doublet scores and
684 predictions. Cells with more than 500 detectable genes with a doublet score of <0.25 and
685 expression of mitochondrial genes accounted for less than 5% of total expression were filtered
686 from the dataset for further downstream analysis. The final dataset includes ESC, ESTS, and
687 TSC derived from blastocysts. Samples were integrated using the merge function in the Seurat
688 suite. Normalization and variance stabilization was done by sctransform and variations due to
689 genes were regressed out. Cells were clustered with the FindClusters function with a resolution
690 of 0.5 and visualization was done using the RunUMAP function.

691 **Data and materials availability:**

692 All the cell lines and plasmid constructs used in this study will be made available against and
693 email request and Material Transfer Agreement (MTA). Raw and processed transcriptome data
694 is deposited in NCBI GEO and is available under the accession GSE219001. The code used for
695 analysis and visualization of scRNAseq data is available at https:
696 https://github.com/SowpatiLab/ES-TSCs

697 **Statistical analysis**

698 Statistical analysis was done by using a two-tailed paired student t-test. The representation of
699 data is in the form of means+/-SDM. The was calculated for more than three independent
700 experiments P value<0.05 is considered statistically significant. * represents P<0.05, **
701 represents P<0.01, *** represents P<0.001, and **** represents P<0.0001.

702

703 **Supplementary Figures**

704 **Supplementary Fig. 1.** (A) q-RTPCR analysis of expression of TE lineage genes at indicated
705 timelines after CHIR treatment. error bar represents the SD of the mean of biological replicates
706 (n=3). '*' indicates a p-value <0.05, '**' indicates a p-value <0.01, 'ns' indicates a p-value >
707 0.05. (B) Expression of Cdx2 transcript in ESCs cultured in indicated combinations and
708 concentration of PD and CHIR relative to ESCs cultured in SL. The error bar represents the
709 SD of the mean of biological replicates (n=3). '*' indicates a p-value <0.05, '**' indicates a p-
710 value <0.01, '***' indicates a p-value <0.001, 'ns' indicates a p-value > 0.05. (C) Relative
711 CDX2 and GATA3 levels as estimated by densitometry. The error bar represents the SD of the
712 mean of biological replicates (n=3). '*' indicates a p-value <0.05, '**' indicates a p-value
713 <0.01, '***' indicates a p-value <0.001, 'ns' indicates a p-value > 0.05. (D) Pie chart indicating

714 the fraction of cells expressing OCT4 or CDX2 or both analyzed from the immunofluorescence
715 data. (E) Schematic depiction of TCMC-OGFP ESC line reporting Cdx2 and Oct4 expression
716 by mCherry and GFP respectively. A T2A-mCherry cassette is integrated in-frame with the last
717 coding sequence of one allele of the Cdx2 gene. An IRES-GFP cassette is integrated into the
718 3'UTR of one of the alleles of the Oct4 gene. (F) FACS profile for TCMC-OGFP ESC line at
719 different time points of CHIR treatment. (G) (Top) Experimental scheme to analyse the ability
720 of the Cdx2 or Oct4 or Cdx2+Oct4 expressing subpopulation of TCMC-OGFP cells to retain
721 or lose the expression of Cdx2 or Oct4 in SL and TSC culture media. The TCMC-OGFP were
722 cultured in SLCHIR for 48hrs and the cells were sorted as Cdx2 mCherry (P1), Cdx2-mCherry
723 + Oct4-GFP (P2), and Oct4-GFP (P3) populations. The sorted cells were cultured in ESC
724 culture media (SL) and TSC media (Tanaka et. al.2005). The cells were analysed for expression
725 of CDX2 and OCT4 by immunostaining after 72 hours of culture. Scale bar = 100µm. (Bottom)
726 Immunofluorescence assay for detection of CDX2 and OCT4 of P1, P2, and P3 subpopulation
727 cells cultured in SL and TSC media. (H) Population of cells expressing CDX2 or OCT4 in
728 subpopulations P1, P2, and P3 after 72hrs of culture in SL or TSC media. '*' indicates a p-
729 value <0.05, '**' indicates a p-value <0.01, '***' indicates a p-value <0.001, '****' indicates
730 a p-value <0.0001 'ns' indicates a p-value > 0.05.

731 **Supplementary Fig. 2.** (A) Bright-field images of ESCs grown under indicated TSC culture
732 conditions. Scale bar =100µm. (B) Flow chart showing the derivation of ESTS from ESC. (C)
733 Phase contrast image of ESCs grown in continuous CHIR treatment in CDM/FAXY media.
734 Scale bar = 100µm. D) (Left) immunoblot analysis of CDX2, GATA3, and ACTIN in TSC and
735 ESTS cells in FAXY containing 5 nM XAV. (Right) Relative CDX2 and GATA3 levels as
736 estimated by densitometry. The error bar represents the SD of the mean of biological replicates
737 (n=3). '*' indicates a p-value <0.05, '**' indicates a p-value <0.01. (E) (Top)
738 Immunofluorescence of CDX2 and OCT4 in TSC and ESTS cultured in CDM/FAXY. (Bottom)
739 Immunofluorescence of GATA3 and OCT4 in TSC and ESTS cultured in CDM/FAXY media.
740 Scale bar = 100µm.

741 **Supplementary Fig. 3.** (A) Principal component analysis (PCA) of RNA-seq of ESC, TSC,
742 and ESTS (B) Heatmap of expression of TE lineage genes from RNA-seq data of ESC, TSC,
743 and ESTS. (C) Heatmap of expression of TE lineage genes from RNA-seq data of ESC, TSC,
744 and ESTS (D) scater plot of the top 10 genes differentially expressed in different clusters of
745 ESC, TSC, and ESTS from sc-RNA seq. (E) Feature plots projecting expression of
746 representative polar and mural markers of TE overlaying in Fig 2A UMAP. (F)

747 Immunofluorescence of GATA3, GFP and OCT4 in E3.5 after injection of GFP labelled ESTS
748 (ESTS-GFP) into 8-cell stage embryo. Scale bar = 50µm (G) Representative image showing
749 the contribution of GFP labelled ESTS descendant cells to the placenta at E12.5 (H)
750 Immunofluorescence of KRT8 and GFP in the E12.5 placental section of ESTS transferred
751 embryo. DC, JZ and LB depict the decidual region, junctional zone, and labyrinth region of the
752 placenta respectively. Scale bar = 2000µm

753 **Supplementary Fig. 4.** (A) Relative CDX2 and NANOG levels in cells cultured in SL and
754 SLCHIR as estimated by densitometry of the indicated cell lines (n=3). B) Relative CDX2 and
755 OCT4 levels in cells cultured in SL and SLCHIR as estimated by densitometry of the indicated
756 cell lines (n=3). '*' indicates a p-value <0.05, '**' indicates a p-value <0.01, '***' indicates a
757 p-value <0.001, 'ns' indicates a p-value > 0.05. (C) Schematic depiction of ZHBTc4 and
758 ZHBTc4 NOE cell lines. (D) Pie chart representing the percentage of the cells expressing
759 CDX2 and NANOG upon doxycycline treatment in ZHB and ZHB NOE cell lines at a different
760 time point of doxycycline treatment. (E) Immunofluorescence of CDX2, NANOG, and OCT4
761 in ZHB and ZHB NOE cell lines treated with or no Doxycycline. (Scale bar = 100µm). (F)
762 Schematic depicting the analysis of ChIP enrichment peaks previously pulled down by OCT4,
763 NANOG, YAP/TAZ, β-CATENIN, and TCF3 on Cdx2 loci by different experiments and
764 groups listed. (G) (Left) Schematic depiction of TCMCβ-Catenin-/-. The cell line was derived
765 from TCMC by CRISPR-mediated knockout of β-Catenin. (Right) histogram profile of
766 mCherry expression in TCMC, TCMC treated with CHIR, and TCMCβ-Cat -/- treated with
767 CHIR.

768 **Supplementary Fig. 5.** (A) Relative expression levels of indicated TE lineage genes Cdx2,
769 Gata3, and Tead4 in ESC cultured in the indicated culture conditions. TSCs were used as a
770 positive control. (B) Contour plots generated from FACS and showing the expression of
771 mCherry in TCMC, TCMCΔTEE, TCMCΔOBR, TCMCNBR, TCMCΔONBR, and
772 TCMCΔIEE cultured in SL and 2iL.

773 **References**

774 Beddington, R., and Robertson, E. (1989). An assessment of the developmental potential of
775 embryonic stem cells in the midgestation mouse embryo. Development *105*, 733-737.
776 Boyer, L.A., Plath, K., Zeitlinger, J., Brambrink, T., Medeiros, L.A., Lee, T.I., Levine, S.S., Wernig, M.,
777 Tajonar, A., and Ray, M.K. (2006). Polycomb complexes repress developmental regulators in murine
778 embryonic stem cells. nature *441*, 349-353.

779 Cambuli, F., Murray, A., Dean, W., Dudzinska, D., Krueger, F., Andrews, S., Senner, C.E., Cook, S.J.,
780 and Hemberger, M. (2014). Epigenetic memory of the first cell fate decision prevents complete ES
781 cell reprogramming into trophoblast. Nature communications *5*, 1-16.
782 Chambers, I., Silva, J., Colby, D., Nichols, J., Nijmeijer, B., Robertson, M., Vrana, J., Jones, K.,
783 Grotewold, L., and Smith, A. (2007). Nanog safeguards pluripotency and mediates germline
784 development. Nature *450*, 1230-1234.
785 Chazaud, C., Yamanaka, Y., Pawson, T., and Rossant, J. (2006). Early lineage segregation between
786 epiblast and primitive endoderm in mouse blastocysts through the Grb2-MAPK pathway.
787 Developmental cell *10*, 615-624.
788 Chen, L., Yabuuchi, A., Eminli, S., Takeuchi, A., Lu, C.-W., Hochedlinger, K., and Daley, G.Q. (2009).
789 Cross-regulation of the Nanog and Cdx2 promoters. Cell research *19*, 1052-1061.
790 Cockburn, K., and Rossant, J. (2010). Making the blastocyst: lessons from the mouse. The Journal of
791 clinical investigation *120*, 995-1003.
792 Dong, C., Beltcheva, M., Gontarz, P., Zhang, B., Popli, P., Fischer, L.A., Khan, S.A., Park, K.-m., Yoon,
793 E.-J., and Xing, X. (2020). Derivation of trophoblast stem cells from naïve human pluripotent stem
794 cells. Elife *9*, e52504.
795 Frias-Aldeguer, J., Kip, M., Vivié, J., Li, L., Alemany, A., Korving, J., Darmis, F., van Oudenaarden, A.,
796 Geijsen, N., and Rivron, N. (2019). Embryonic signals perpetuate polar-like trophoblast stem cells
797 and pattern the blastocyst axis.
798 Gardner, R. (1983). Origin and differentiation of extraembryonic tissues in the mouse. Int Rev Exp
799 Pathol *24*, 63-133.
800 Gardner, R., and Rossant, J. (1979). Investigation of the fate of 4· 5 day post-coitum mouse inner cell
801 mass cells by blastocyst injection.
802 Guo, G., Stirparo, G.G., Strawbridge, S.E., Spindlow, D., Yang, J., Clarke, J., Dattani, A., Yanagida, A.,
803 Li, M.A., and Myers, S. (2021). Human naive epiblast cells possess unrestricted lineage potential. Cell
804 stem cell *28*, 1040-1056. e1046.
805 Hao, J., Li, T.-G., Qi, X., Zhao, D.-F., and Zhao, G.-Q. (2006). WNT/β-catenin pathway up-regulates
806 Stat3 and converges on LIF to prevent differentiation of mouse embryonic stem cells. Developmental
807 biology *290*, 81-91.
808 Huang, S.-M.A., Mishina, Y.M., Liu, S., Cheung, A., Stegmeier, F., Michaud, G.A., Charlat, O.,
809 Wiellette, E., Zhang, Y., and Wiessner, S. (2009). Tankyrase inhibition stabilizes axin and antagonizes
810 Wnt signalling. Nature *461*, 614-620.
811 Jaber, M., Radwan, A., Loyfer, N., Abdeen, M., Sebban, S., Khatib, A., Yassen, H., Kolb, T., Zapatka,
812 M., and Makedonski, K. (2022). Comparative parallel multi-omics analysis during the induction of
813 pluripotent and trophectoderm states. Nature Communications *13*, 3475.
814 Jana, D., Kale, H.T., and Shekar, P.C. (2019). Generation of Cdx2-mCherry knock-in murine ES cell line
815 to model trophectoderm and intestinal lineage differentiation. Stem cell research *39*, 101521.
816 Jana, D., Singh, P., Sailasree, P., Kumar, N., Vijay, V., Kale, H., Lakshmi, J., Kumari, A., Sowpati, D.T.,
817 and Shekar, C. (2023). Efficient self-organization of blastoids solely from mouse ESCs is facilitated by
818 transient reactivation of 2C gene network. bioRxiv, 2023.2004. 2012.536583.
819 Jang, Y.J., Kim, M., Lee, B.-K., and Kim, J. (2022). Induction of human trophoblast stem-like cells from
820 primed pluripotent stem cells. Proceedings of the National Academy of Sciences *119*, e2115709119.
821 Kagawa, H., Javali, A., Khoei, H.H., Sommer, T.M., Sestini, G., Novatchkova, M., Scholte op Reimer, Y.,
822 Castel, G., Bruneau, A., and Maenhoudt, N. (2022). Human blastoids model blastocyst development
823 and implantation. Nature *601*, 600-605.
824 Kale, H.T., Rajpurohit, R.S., Jana, D., Vishnu, V.V., Srivastava, M., Mourya, P.R., Srinivas, G., and
825 Shekar, P.C. (2022). A NANOG-pERK reciprocal regulatory circuit regulates Nanog autoregulation and
826 ERK signaling dynamics. EMBO reports *23*, e54421.
827 Kuckenberg, P., Buhl, S., Woynecki, T., van Fürden, B., Tolkunova, E., Seiffe, F., Moser, M., Tomilin,
828 A., Winterhager, E., and Schorle, H. (2010). The transcription factor TCFAP2C/AP-2γ cooperates with
829 CDX2 to maintain trophectoderm formation. Molecular and cellular biology *30*, 3310-3320.

830 Li, J., Zhu, Q., Cao, J., Liu, Y., Lu, Y., Sun, Y., Li, Q., Huang, Y., Shang, S., and Bian, X. (2023).
831 Cynomolgus monkey embryo model captures gastrulation and early pregnancy. Cell Stem Cell *30*,
832 362-377. e367.
833 Li, Y., Moretto-Zita, M., Soncin, F., Wakeland, A., Wolfe, L., Leon-Garcia, S., Pandian, R., Pizzo, D., Cui,
834 L., and Nazor, K. (2013). BMP4-directed trophoblast differentiation of human embryonic stem cells is
835 mediated through a ΔNp63+ cytotrophoblast stem cell state. Development *140*, 3965-3976.
836 Liang, W., Li, G., Cui, H., Wang, Y., Wei, W., Sun, S., Gan, D., Chen, R., Yi, H., and Schaefke, B. (2021).
837 Evolutionary Analysis of Transcriptional Regulation Mediated by Cdx2 in Rodents. bioRxiv.
838 Marchand, M., Horcajadas, J.A., Esteban, F.J., McElroy, S.L., Fisher, S.J., and Giudice, L.C. (2011).
839 Transcriptomic signature of trophoblast differentiation in a human embryonic stem cell model.
840 Biology of reproduction *84*, 1258-1271.
841 Murray, A., Sienerth, A.R., and Hemberger, M. (2016). Plet1 is an epigenetically regulated cell surface
842 protein that provides essential cues to direct trophoblast stem cell differentiation. Scientific Reports
843 *6*, 1-14.
844 Ng, R.K., Dean, W., Dawson, C., Lucifero, D., Madeja, Z., Reik, W., and Hemberger, M. (2008).
845 Epigenetic restriction of embryonic cell lineage fate by methylation of Elf5. Nature cell biology *10*,
846 1280-1290.
847 Nichols, J., and Gardner, R. (1984). Heterogeneous differentiation of external cells in individual
848 isolated early mouse inner cell masses in culture.
849 Nishioka, N., Inoue, K.-i., Adachi, K., Kiyonari, H., Ota, M., Ralston, A., Yabuta, N., Hirahara, S.,
850 Stephenson, R.O., and Ogonuki, N. (2009). The Hippo signaling pathway components Lats and Yap
851 pattern Tead4 activity to distinguish mouse trophectoderm from inner cell mass. Developmental cell
852 *16*, 398-410.
853 Niwa, H., Miyazaki, J.-i., and Smith, A.G. (2000). Quantitative expression of Oct-3/4 defines
854 differentiation, dedifferentiation or self-renewal of ES cells. Nature genetics *24*, 372-376.
855 Niwa, H., Toyooka, Y., Shimosato, D., Strumpf, D., Takahashi, K., Yagi, R., and Rossant, J. (2005).
856 Interaction between Oct3/4 and Cdx2 determines trophectoderm differentiation. Cell *123*, 917-929.
857 Ohinata, Y., and Tsukiyama, T. (2014). Establishment of trophoblast stem cells under defined culture
858 conditions in mice. PloS one *9*, e107308.
859 Okae, H., Toh, H., Sato, T., Hiura, H., Takahashi, S., Shirane, K., Kabayama, Y., Suyama, M., Sasaki, H.,
860 and Arima, T. (2018). Derivation of human trophoblast stem cells. Cell stem cell *22*, 50-63. e56.
861 Plusa, B., Piliszek, A., Frankenberg, S., Artus, J., and Hadjantonakis, A.-K. (2008). Distinct sequential
862 cell behaviours direct primitive endoderm formation in the mouse blastocyst.
863 Posfai, E., Petropoulos, S., de Barros, F.R.O., Schell, J.P., Jurisica, I., Sandberg, R., Lanner, F., and
864 Rossant, J. (2017). Position-and Hippo signaling-dependent plasticity during lineage segregation in
865 the early mouse embryo. Elife *6*, e22906.
866 Posfai, E., Schell, J.P., Janiszewski, A., Rovic, I., Murray, A., Bradshaw, B., Yamakawa, T., Pardon, T., El
867 Bakkali, M., and Talon, I. (2021). Evaluating totipotency using criteria of increasing stringency.
868 Nature cell biology *23*, 49-60.
869 Ralston, A., Cox, B.J., Nishioka, N., Sasaki, H., Chea, E., Rugg-Gunn, P., Guo, G., Robson, P., Draper,
870 J.S., and Rossant, J. (2010). Gata3 regulates trophoblast development downstream of Tead4 and in
871 parallel to Cdx2. Development *137*, 395-403.
872 Solter, D., and Knowles, B.B. (1975). Immunosurgery of mouse blastocyst. Proceedings of the
873 National Academy of Sciences *72*, 5099-5102.
874 Tanaka, S. (2006). Derivation and culture of mouse trophoblast stem cells in vitro. In Embryonic Stem
875 Cell Protocols (Springer), pp. 35-44.
876 Wei, Y., Wang, T., Ma, L., Zhang, Y., Zhao, Y., Lye, K., Xiao, L., Chen, C., Wang, Z., and Ma, Y. (2021).
877 Efficient derivation of human trophoblast stem cells from primed pluripotent stem cells. Science
878 Advances *7*, eabf4416.
879 Yang, J., Ryan, D.J., Wang, W., Tsang, J.C.-H., Lan, G., Masaki, H., Gao, X., Antunes, L., Yu, Y., and Zhu,
880 Z. (2017a). Establishment of mouse expanded potential stem cells. Nature *550*, 393-397.

Yang, Y., Liu, B., Xu, J., Wang, J., Wu, J., Shi, C., Xu, Y., Dong, J., Wang, C., and Lai, W. (2017b). Derivation of pluripotent stem cells with in vivo embryonic and extraembryonic potency. Cell *169*, 243-257. e225.

Ying, Q.-L., Wray, J., Nichols, J., Batlle-Morera, L., Doble, B., Woodgett, J., Cohen, P., and Smith, A. (2008). The ground state of embryonic stem cell self-renewal. nature *453*, 519-523.

Zijlmans, D.W., Talon, I., Verhelst, S., Bendall, A., Van Nerum, K., Javali, A., Malcolm, A.A., van Knippenberg, S.S., Biggins, L., and To, S.K. (2022). Integrated multi-omics reveal polycomb repressive complex 2 restricts human trophoblast induction. Nature cell biology *24*, 858-871.

Zita, M.M., Soncin, F., Natale, D., Pizzo, D., and Parast, M. (2015). Gene expression profiling reveals a novel regulatory role for Sox21 protein in mouse trophoblast stem cell differentiation. Journal of Biological Chemistry *290*, 30152-30162.

Figure 1

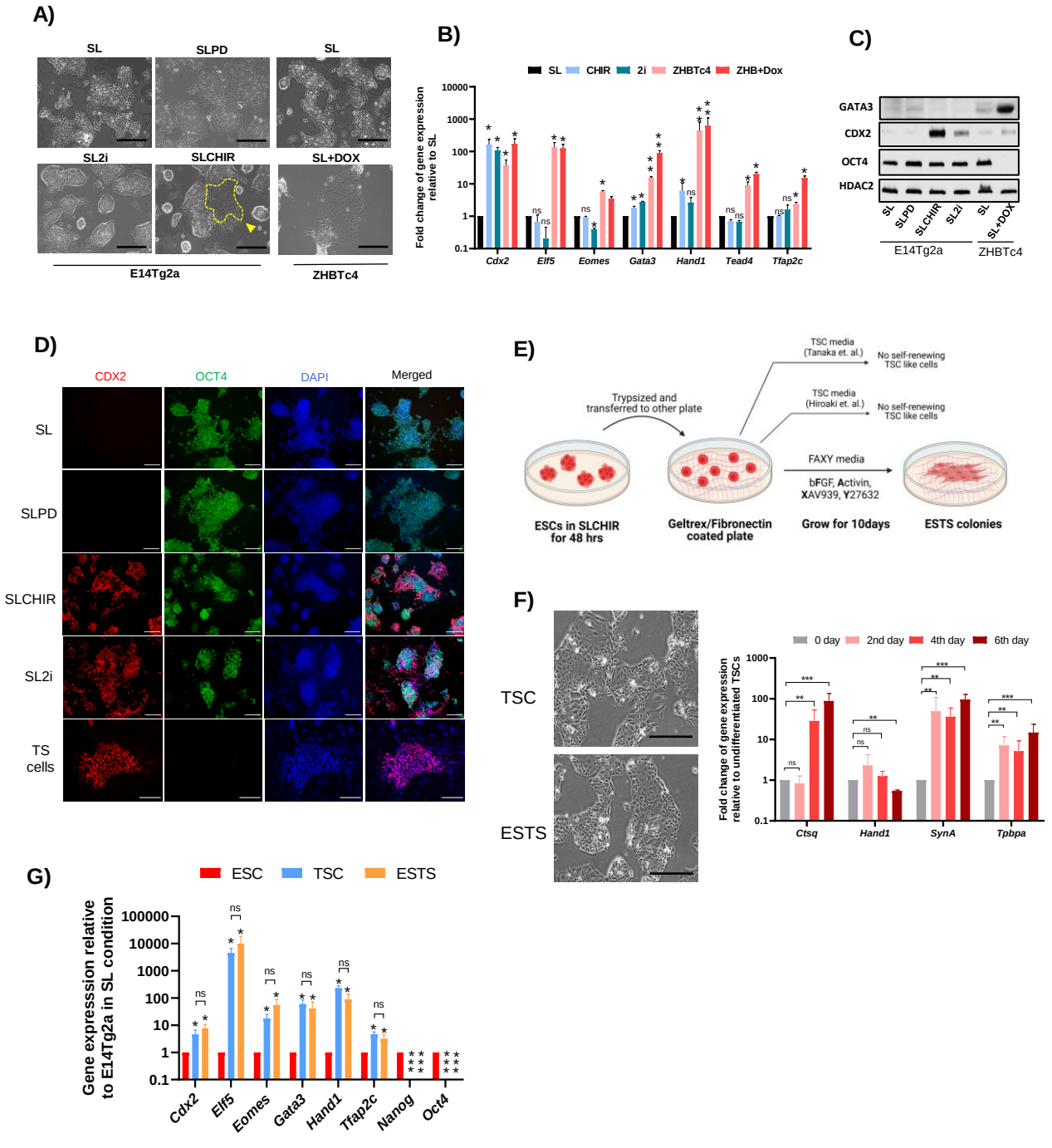
A)
SL
SLPD
SL
SL2i
SLCHIR
SL+DOX
E14Tg2a
ZHBTc4
B)
SL
CHIR
2i
ZHBTc4
ZHB+Dox
Fold change of gene expression relative to SL
Cdx2
Elf5
Eomes
Gata3
Hand1
Tead4
Tfap2c
C)
GATA3
CDX2
OCT4
HDAC2
SL
SLPD
SLCHIR
SL2i
SL
SL+DOX
E14Tg2a
ZHBTc4
D)
CDX2
OCT4
DAPI
Merged
SL
SLPD
SLCHIR
SL2i
TS cells
E)
Trypsized and transferred to other plate
TSC media (Tanaka et. al.)
No self-renewing TSC like cells
TSC media (Hiroaki et. al.)
No self-renewing TSC like cells
FAXY media
bFGF, Activin, XAV939, Y27632
ESCs in SLCHIR for 48 hrs
Geltrex/Fibronectin coated plate
Grow for 10days
ESTS colonies
F)
TSC
ESTS
0 day
2nd day
4th day
6th day
Fold change of gene expression relative to undifferentiated TSCs
Ctsq
Hand1
SynA
Tpbpa
G)
ESC
TSC
ESTS
Gene expresssion relative to E14Tg2a in SL condition
Cdx2
Elf5
Eomes
Gata3
Hand1
Tfap2c
Nanog
Oct4

Figure 2

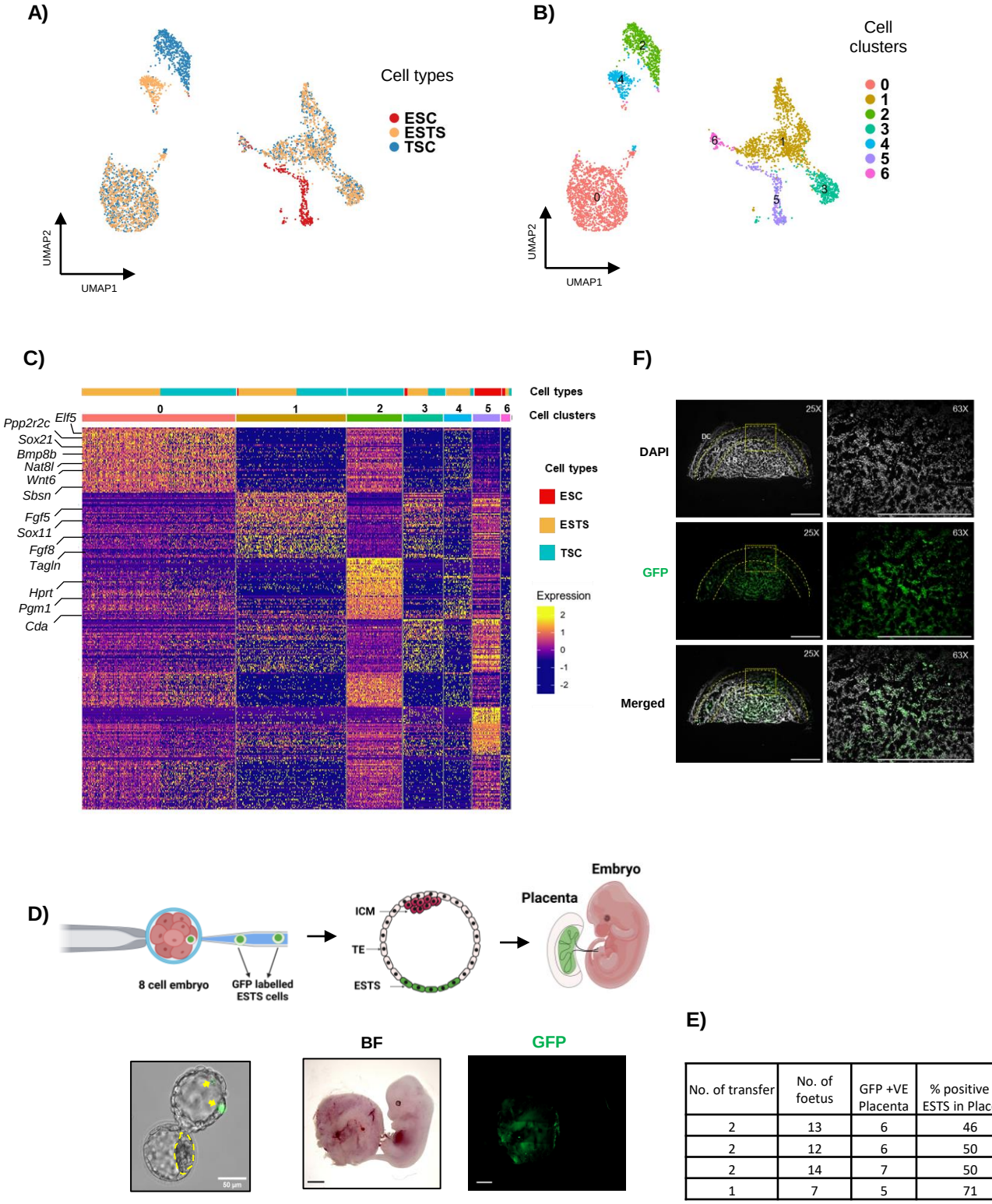

E)

No. of transfer	No. of foetus	GFP +VE Placenta	% positive for ESTS in Placenta
2	13	6	46
2	12	6	50
2	14	7	50
1	7	5	71

Figure 3

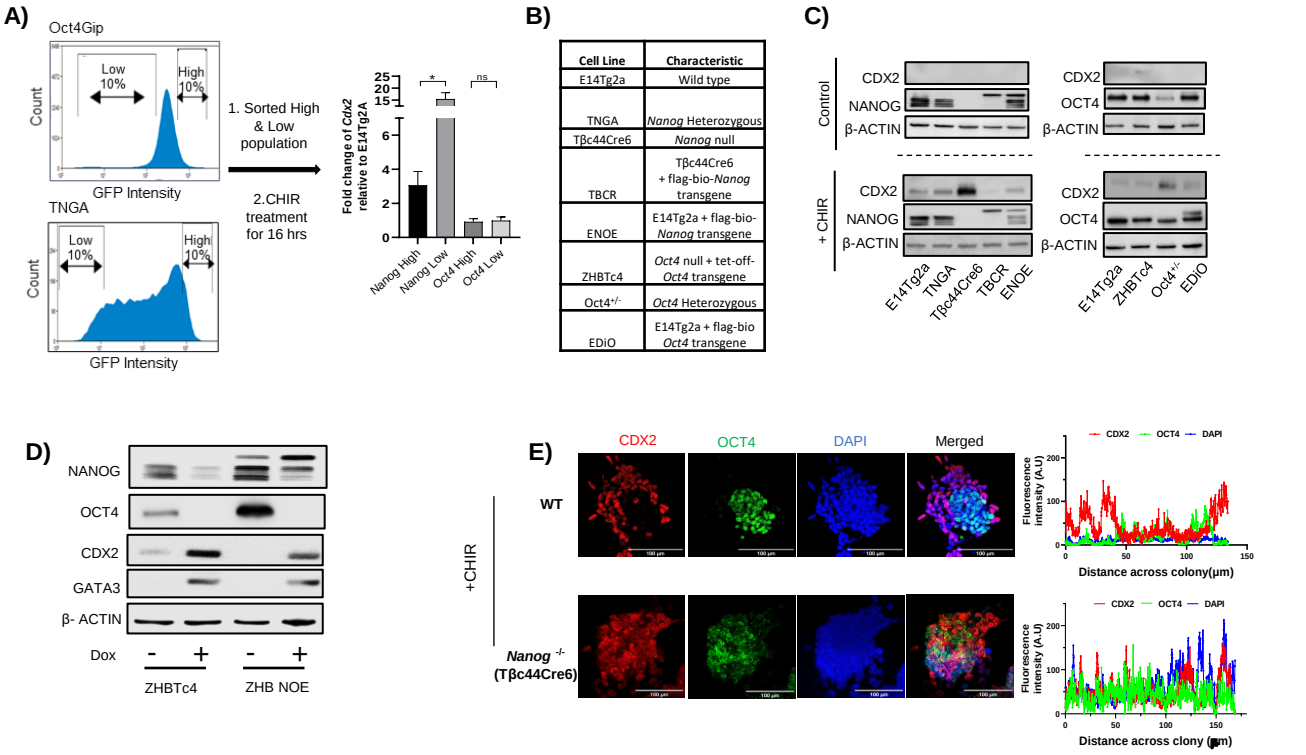
A)
Oct4Gip
Low 10%
High 10%
Count
GFP Intensity
TNGA
1. Sorted High & Low population
2.CHIR treatment for 16 hrs
Fold change of Cdx2 relative to E14Tg2A
Nanog High
Nanog Low
Oct4 High
Oct4 Low
B)
Cell Line | Characteristic
E14Tg2a | Wild type
TNGA | Nanog Heterozygous
Tβc44Cre6 | Nanog null
TBCR | Tβc44Cre6 + flag-bio-Nanog transgene
ENOE | E14Tg2a + flag-bio-Nanog transgene
ZHBTc4 | Oct4 null + tet-off-Oct4 transgene
Oct4+/- | Oct4 Heterozygous
EDiO | E14Tg2a + flag-bio Oct4 transgene
C)
Control
+ CHIR
CDX2
NANOG
OCT4
β-ACTIN
E14Tg2a
TNGA
Tβc44Cre6
TBCR
ENOE
ZHBTc4
Oct4+/-
EDiO
D)
NANOG
OCT4
CDX2
GATA3
β- ACTIN
Dox
ZHBTc4
ZHB NOE
E)
CDX2
OCT4
DAPI
Merged
WT
+CHIR
Nanog -/- (Tβc44Cre6)
Fluorescence intensity (A.U)
Distance across colony(μm)
Distance across clony (μm)
F)
Element of interest
Minimal β-globin promoter
mCherry
Untreated
+CHIR
TSS reporter
Intron 1 reporter
TEE reporter
Count
mCherry
G) Cdx2-mCherry locus
mCherry
3' UTR
SL
SLCHIR
WT TCMC
TCMC ΔTEE
TCMC ΔOBR
TCMC ΔNBR
TCMC ΔONBR
TCMC ΔIEE
26%
24%
2%
1%
4%
24%
mCherry
FL1

Figure 4

A)

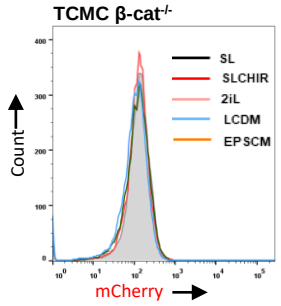

B)

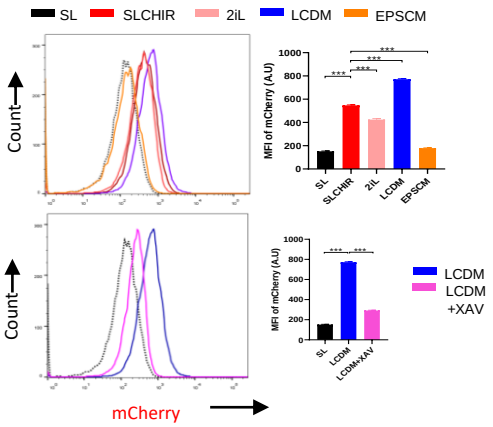

C)

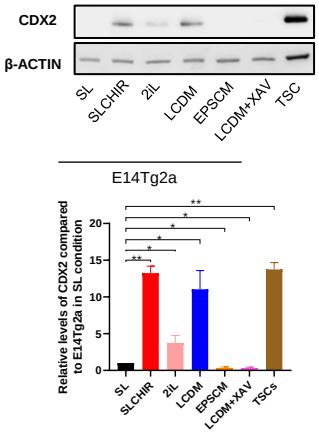

D)

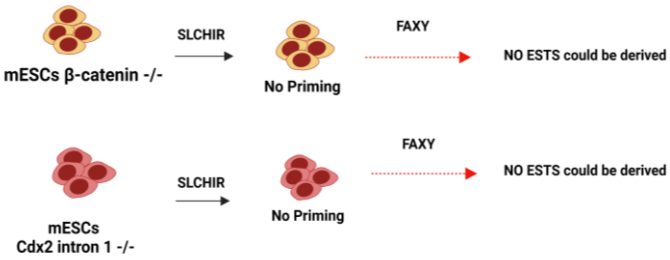

E)

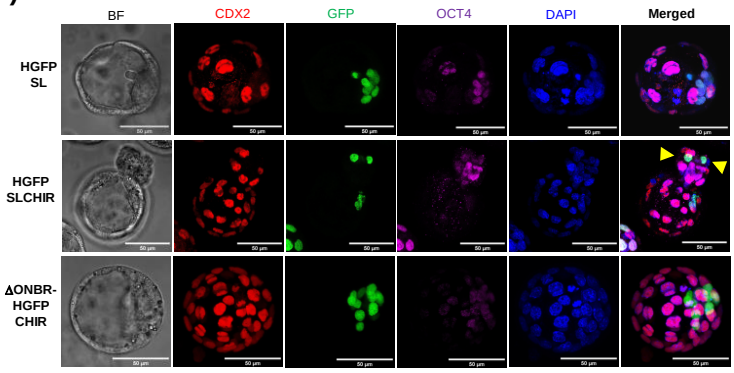

Cell type injected	Injected cells condition	Contribution to TE (outer layers)	GFP co-stained with CDX2 in outer layers
HGFP	SL	0/33	-
	SLCHIR	5/67 (7%)	0/5
HGFP ΔONBR	SLCHIR	0/70	-

F)

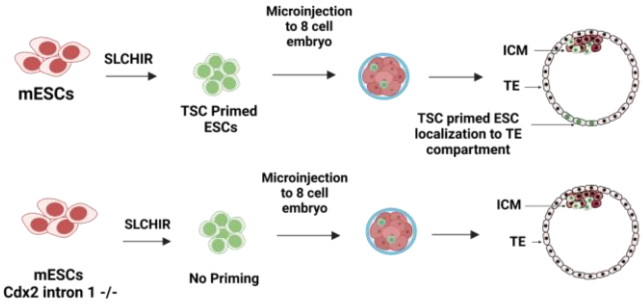

Figure 5

A)

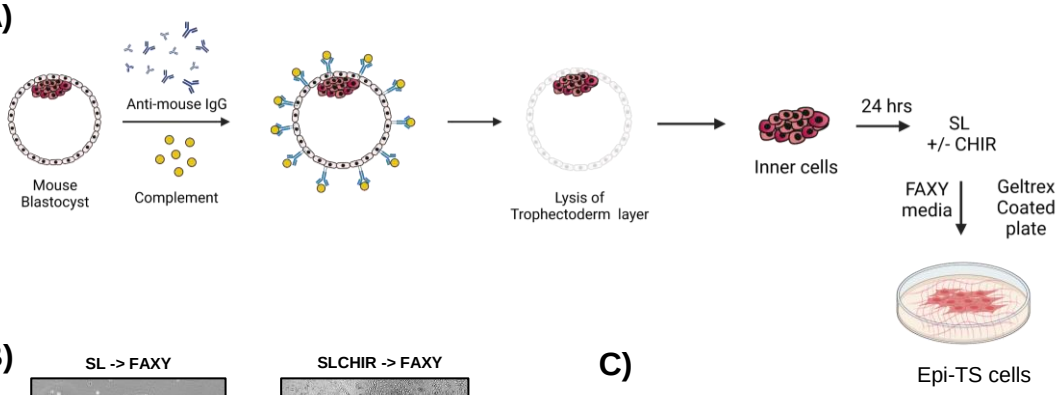

B)

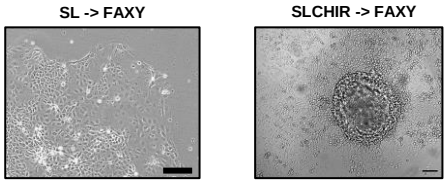

C)

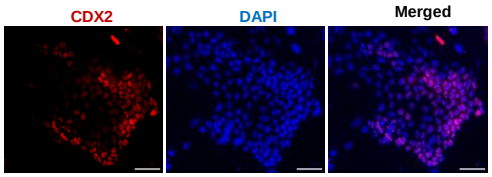

D)

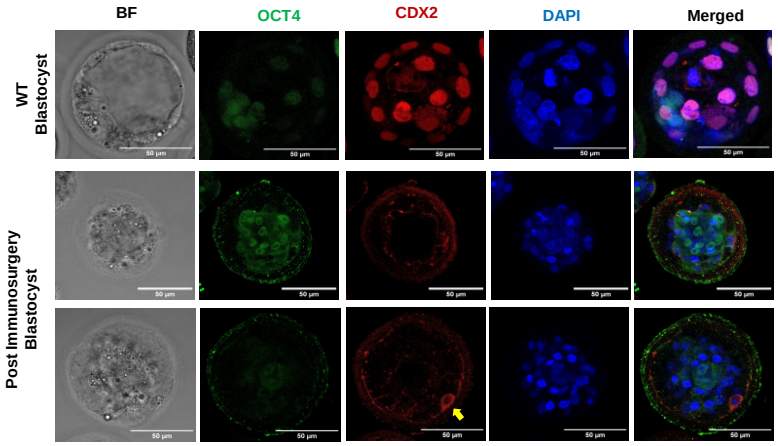

E)

No. of embryos screened	No. of embryos having CDX2 expressing cell after Immunosurgery	No. of TS outgrowth after immunosurgery
96	1/48 (2%)	8/48 (16%)

F)

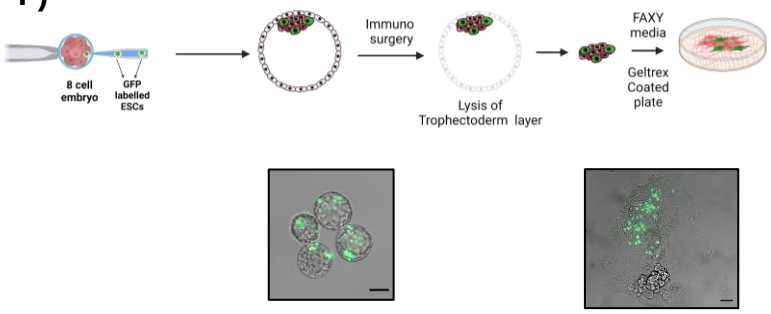

G)

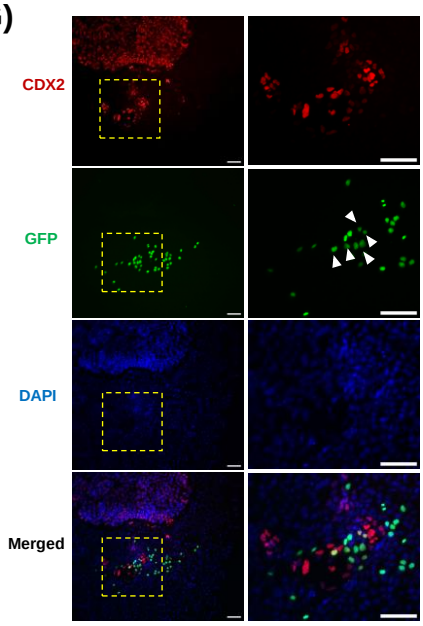

No. of HGFP injected embryos	No. of outgrowth having GFP cells co- expressing CDX2
20	4/20 (20%)

Fig. S1

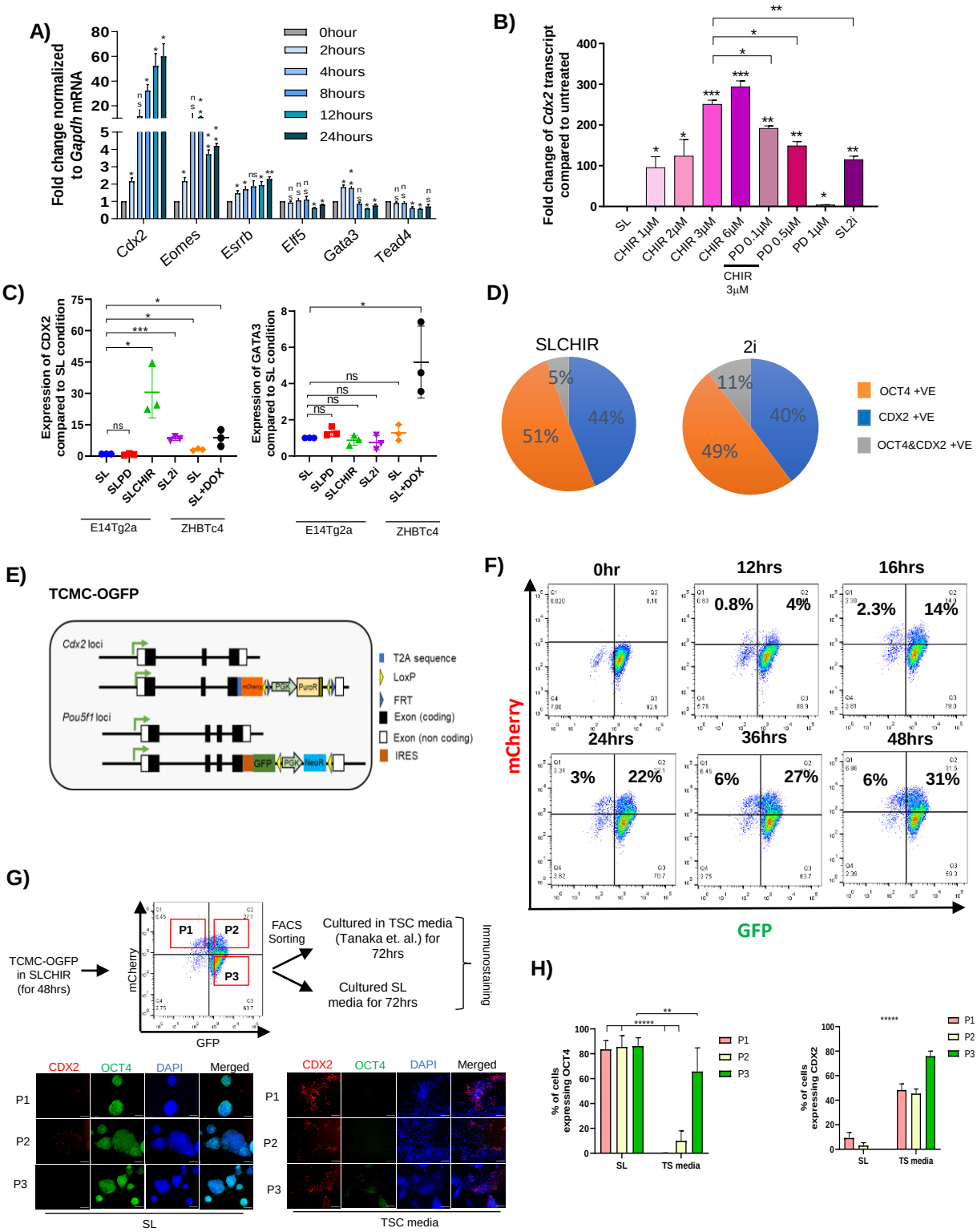
A)
Fold change normalized to Gapdh mRNA
0hour
2hours
4hours
8hours
12hours
24hours
Cdx2
Eomes
Esrrb
Elf5
Gata3
Tead4
B)
Fold change of Cdx2 transcript compared to untreated
SL
CHIR 1μM
CHIR 2μM
CHIR 3μM
CHIR 6μM
PD 0.1μM
PD 0.5μM
PD 1μM
SL2i
CHIR 3μM
C)
Expression of CDX2 compared to SL condition
Expression of GATA3 compared to SL condition
SL
SLPD
SLCHIR
SL2i
SL
SL+DOX
E14Tg2a
ZHBTc4
D)
SLCHIR
2i
5%
44%
51%
11%
40%
49%
OCT4 +VE
CDX2 +VE
OCT4&CDX2 +VE
E)
TCMC-OGFP
Cdx2 loci
Pou5f1 loci
T2A sequence
LoxP
FRT
Exon (coding)
Exon (non coding)
IRES
F)
0hr
12hrs
16hrs
24hrs
36hrs
48hrs
0.8%
4%
2.3%
14%
3%
22%
6%
27%
6%
31%
mCherry
GFP
G)
TCMC-OGFP in SLCHIR (for 48hrs)
P1
P2
P3
FACS Sorting
Cultured in TSC media (Tanaka et. al.) for 72hrs
Cultured SL media for 72hrs
Immunostaining
CDX2
OCT4
DAPI
Merged
SL
TSC media
H)
% of cells expressing OCT4
% of cells expressing CDX2
SL
TS media

Fig.S2

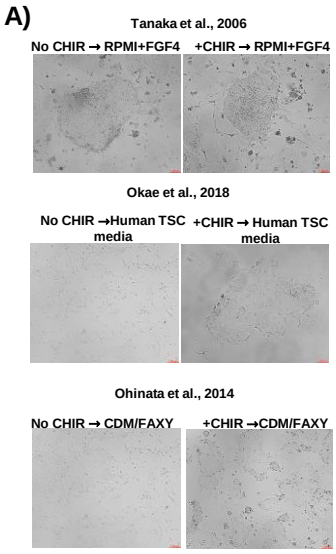
A)
Tanaka et al., 2006
No CHIR → RPMI+FGF4
+CHIR → RPMI+FGF4
Okae et al., 2018
No CHIR →Human TSC media
+CHIR → Human TSC media
Ohinata et al., 2014
No CHIR → CDM/FAXY
+CHIR →CDM/FAXY

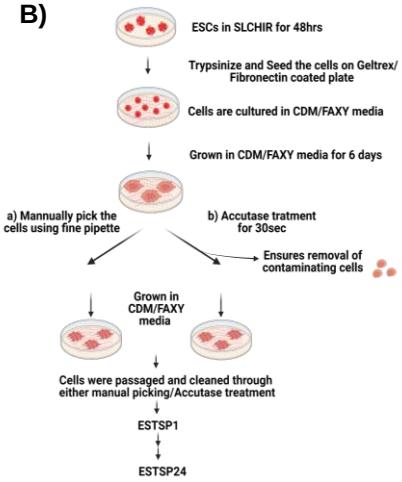
B)
ESCs in SLCHIR for 48hrs
Trypsinize and Seed the cells on Geltrex/ Fibronectin coated plate
Cells are cultured in CDM/FAXY media
Grown in CDM/FAXY media for 6 days
a) Mannually pick the cells using fine pipette
b) Accutase tratment for 30sec
Ensures removal of contaminating cells
Grown in CDM/FAXY media
Cells were passaged and cleaned through either manual picking/Accutase treatment
ESTSP1
ESTSP24

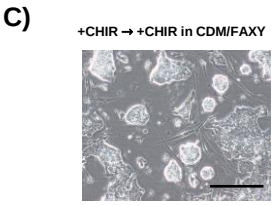
C)
+CHIR → +CHIR in CDM/FAXY

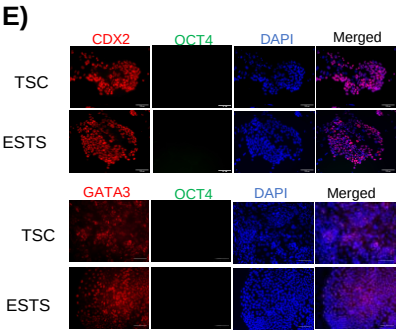
E)
CDX2
OCT4
DAPI
Merged
TSC
ESTS
GATA3
OCT4
DAPI
Merged
TSC
ESTS

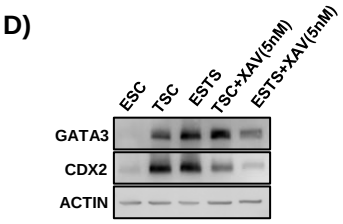
D)
ESC
TSC
ESTS
TSC+XAV(5nM)
ESTS+XAV(5nM)
GATA3
CDX2
ACTIN

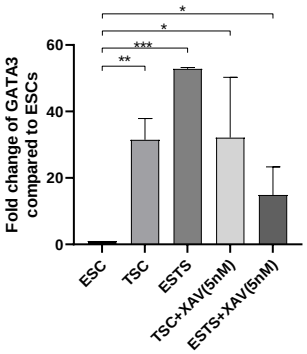
Fold change of GATA3 compared to ESCs
0
20
40
60
**
***
*
*
ESC
TSC
ESTS
TSC+XAV(5nM)
ESTS+XAV(5nM)

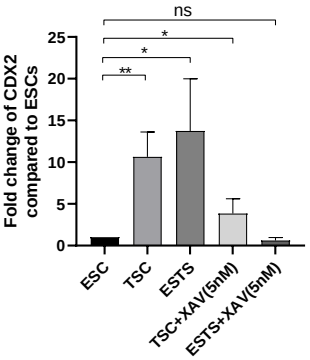
Fold change of CDX2 compared to ESCs
0
5
10
15
20
25
**
*
*
ns
ESC
TSC
ESTS
TSC+XAV(5nM)
ESTS+XAV(5nM)

Fig.S3

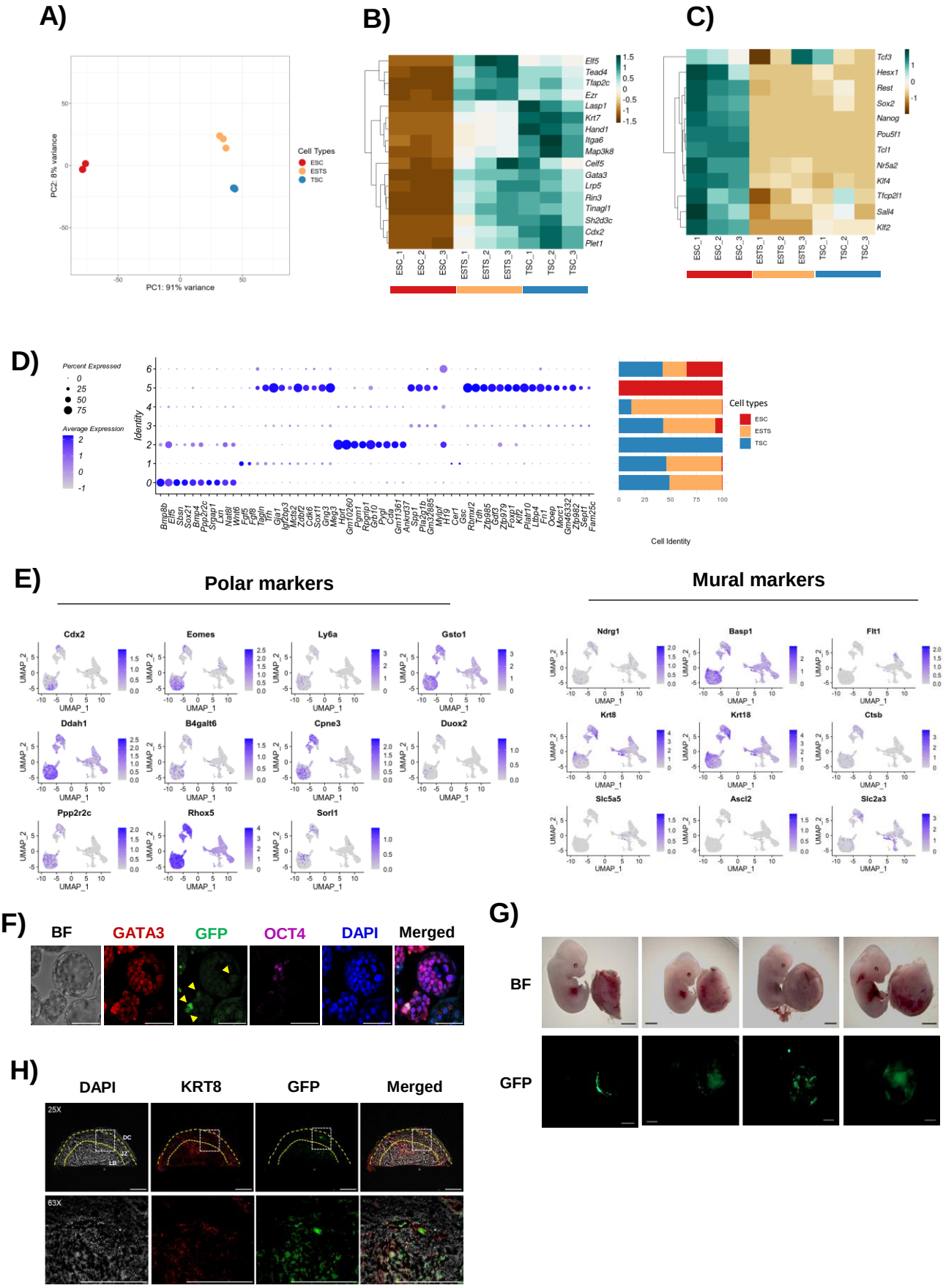
A)
PC2: 8% variance
PC1: 91% variance
Cell Types
ESC
ESTS
TSC
B)
Elf5
Tead4
Tfap2c
Ezr
Lasp1
Krt7
Hand1
Itga6
Map3k8
Celf5
Gata3
Lrp5
Rin3
Tinagl1
Sh2d3c
Cdx2
Plet1
ESC_1
ESC_2
ESC_3
ESTS_1
ESTS_2
ESTS_3
TSC_1
TSC_2
TSC_3
C)
Tcf3
Hesx1
Rest
Sox2
Nanog
Pou5f1
Tcl1
Nr5a2
Klf4
Tfcp2l1
Sall4
Klf2
D)
Percent Expressed
Average Expression
Identity
Cell types
ESC
ESTS
TSC
Cell Identity
E)
Polar markers
Mural markers
Cdx2
Eomes
Ly6a
Gsto1
Ddah1
B4galt6
Cpne3
Duox2
Ppp2r2c
Rhox5
Sorl1
Ndrg1
Basp1
Flt1
Krt8
Krt18
Ctsb
Slc5a5
Ascl2
Slc2a3
UMAP_1
UMAP_2
F)
BF
GATA3
GFP
OCT4
DAPI
Merged
G)
BF
GFP
H)
DAPI
KRT8
GFP
Merged
25X
63X
DC
SZ
LB

Fig. S4

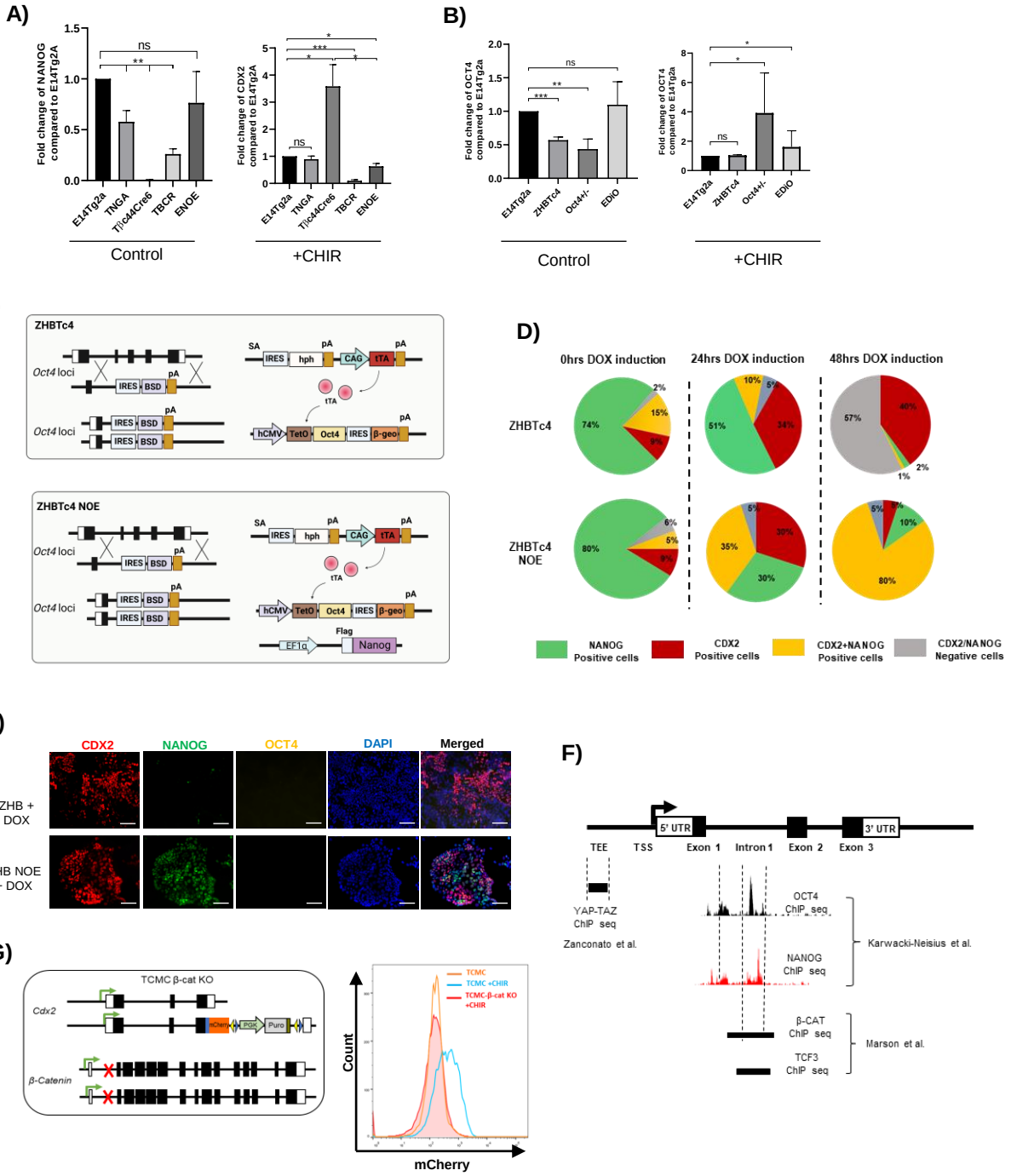
A)
Fold change of NANOG compared to E14Tg2A
Fold change of CDX2 compared to E14Tg2A
E14Tg2a
TNGA
Tlx44Cre6
TBCR
ENOE
Control
+CHIR
B)
Fold change of OCT4 compared to E14Tg2a
E14Tg2a
ZHBTc4
Oct4+/-
EDIO
Control
+CHIR
C)
ZHBTc4
Oct4 loci
IRES
BSD
pA
SA
hph
CAG
tTA
hCMV
TetO
Oct4
β-geo
ZHBTc4 NOE
Flag
EF1α
Nanog
D)
0hrs DOX induction
24hrs DOX induction
48hrs DOX induction
ZHBTc4
ZHBTc4 NOE
NANOG Positive cells
CDX2 Positive cells
CDX2+NANOG Positive cells
CDX2/NANOG Negative cells
E)
CDX2
NANOG
OCT4
DAPI
Merged
ZHB + DOX
ZHB NOE + DOX
F)
5' UTR
3' UTR
TEE
TSS
Exon 1
Intron 1
Exon 2
Exon 3
YAP-TAZ ChIP seq
Zanconato et al.
OCT4 ChIP seq
NANOG ChIP seq
Karwacki-Neisius et al.
β-CAT ChIP seq
TCF3 ChIP seq
Marson et al.
G)
TCMC β-cat KO
Cdx2
β-Catenin
mCherry
PGK
Puro
TCMC
TCMC +CHIR
TCMC-β-cat KO +CHIR
Count
mCherry

Figure S5

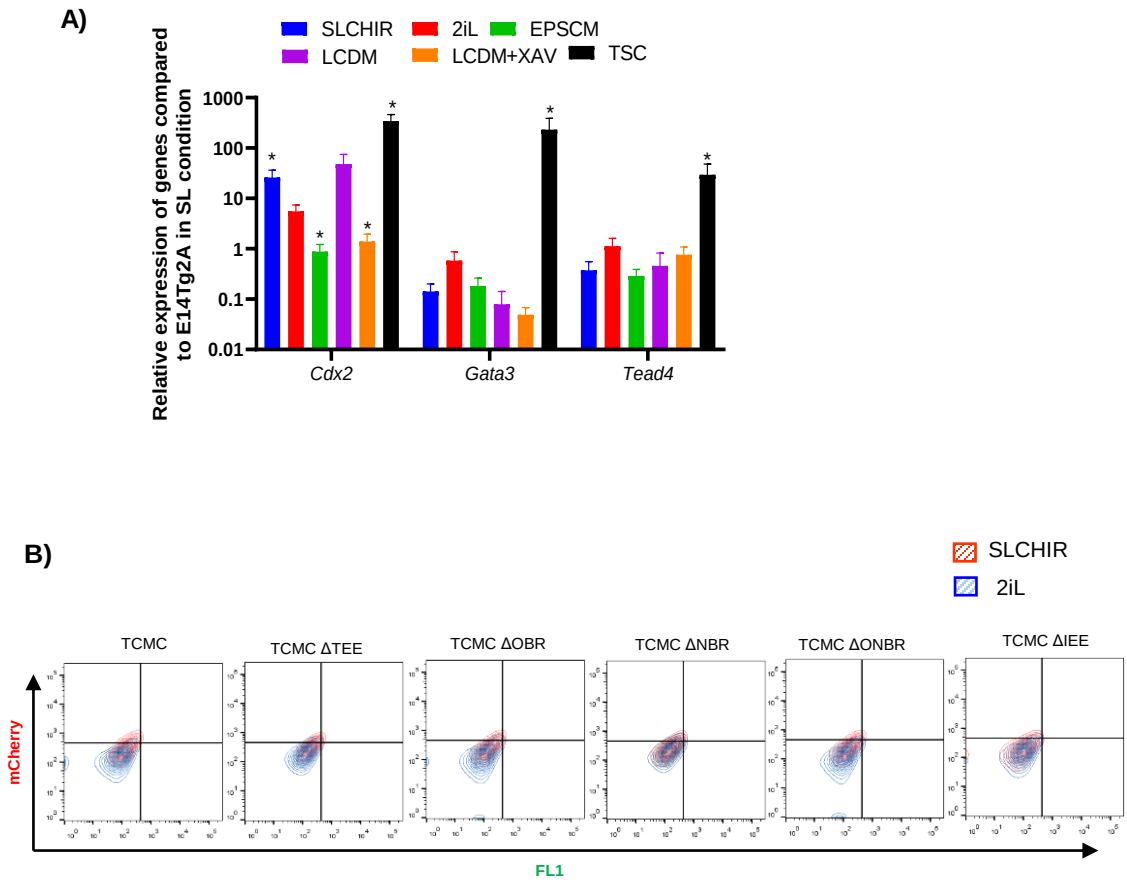
A)
SLCHIR
2iL
EPSCM
LCDM
LCDM+XAV
TSC
Relative expression of genes compared to E14Tg2A in SL condition
1000
100
10
1
0.1
0.01
Cdx2
Gata3
Tead4
B)
SLCHIR
2iL
TCMC
TCMC ΔTEE
TCMC ΔOBR
TCMC ΔNBR
TCMC ΔONBR
TCMC ΔIEE
mCherry
FL1

Key resource table

Resource	Source	Identifier	Dilution/ Temp	Incubation time
Primary Antibodies				
Goat OCT4	Sigma life science	Cat# SAB2500713; RRID: AB_10605123	1:1000; 4 degree	O/N
Mouse beta-actin	Sigma life science	Cat# A5441; RRID: AB_476744	1:1000; 4 degree	O/N
Mouse OCT-3/4 (C-10)	Santa Cruz Biotechnology	Cat# sc-5279; RRID: AB_628051	1:1000; 4 degree	O/N
Goat GATA3	R&D Systems	Cat# AF2606; RRID: AB_2108571	1:1000; 4 degree	O/N
Rabbit β-CATENIN	Cell Signaling Technology	Cat# 8480S; RRID: AB_11127855	1:2000; 4 degree	O/N
Rabbit GATA3	Cell Signaling Technology	Cat# 5852, RRID: AB_10835690	1:2000; 4 degree	O/N
Rabbit NANOG	Cell signaling Technology	Cat# 8822; RRID: AB_11217637	1:2000; 4 degree	O/N
Rabbit HDAC2	Thermo Fisher Scientific	Cat# 51-5100; RRID: AB_2533908	1:1000; 4 degree	O/N
Rabbit CDX2	Thermo Fisher Scientific	Cat# MA5-14494; AB_11004783	1:1000; 4 degree	O/N
Rat NANOG	Thermo Fisher Scientific	Cat# 14-5761-80; RRID: AB_763613	1:1000; 4 degree	O/N
Rabbit GFP	Cell Signaling Technology	Cat# 2555; RRID: AB_10692764	1:1000; 4 degree	O/N
Secondary antibodies				
Donkey anti-Mouse IgG Alexa fluor plus 594	Thermo Fisher Scientific	Cat# A32744; RRID: AB_2762826	1:1000; RT	1 hour
Donkey anti-Mouse IgG Alexa fluor plus 647	Thermo Fisher Scientific	Cat# A32787; RRID: AB_2762830	1:1000; RT	1 hour
Donkey anti-Mouse IgG Alexa fluor plus 488	Thermo Fisher Scientific	Cat# A32766; RRID: AB_2762823	1:1000; RT	1 hour

Donkey anti-Rabbit IgG Alexa fluor plus 647	Thermo Fisher Scientific	Cat# A32795; RRID: AB_2762835	1:1000; RT	1 hour
Chicken anti-rabbit IgG Alexa fluor 488	Thermo Fisher Scientific	Cat# A21441; RRID: AB_2535859	1:1000; RT	1 hour
Chicken anti-rabbit IgG Alexa fluor 594	Thermo Fisher Scientific	Cat# A21442; RRID: AB_141840	1:1000; RT	1 hour
Donkey anti-rat IgG Alexa fluor 488	Thermo Fisher Scientific	Cat# A21208; RRID: AB_141709	1:1000; RT	1 hour
Chicken anti-rat IgG Alexa fluor 647	Thermo Fisher Scientific	Cat# A21472; RRID: AB_1500700	1:1000; RT	1 hour
Chicken anti-goat IgG Alexa fluor 488	Thermo Fisher Scientific	Cat# A21467; RRID: AB_141893	1:1000; RT	1 hour
Chicken anti-goat IgG Alexa fluor 647	Thermo Fisher Scientific	Cat# A21469; RRID: AB_1500603	1:1000; RT	1 hour
Donkey anti-goat IgG Alexa fluor 594	Thermo Fisher Scientific	Cat# A-11058; RRID: AB_2534105	1:1000; RT	1 hour
Donkey anti-Rat HRP	Thermo Fisher Scientific	Cat# A18747, RRID: AB_2535524	1:10000; RT	1 hour
Donkey anti-Rabbit HRP	Sigma life science	Cat# AP182P, RRID: AB_92591	1:10000; RT	1 hour
Donkey anti-Goat HRP	Sigma life science	Cat# AP180P, RRID: AB_92573	1:10000; RT	1 hour

Chemicals, Peptides, and Recombinant Proteins

Resource/Reagent	Source	Identifier
CHIR99021	Sigma life science	Cat# SML1046; lot# 017M4717V
PD325901	Sigma life science	Cat# PZ0162
(S)-(+)-Dimethindene maleate	Tocris bioscience	Cat# 1425; lot# 1A/208761
Minocycline hydrochloride	EMD Millipore	Cat# 475843; lot# 2976370
JNK inhibitor VIII	Santa Cruz Biotechnology	Cat# sc-202673; lot# H1919
A83-01	Sigma life science	Cat# SML0788; lot# 0000073372
SB 203580	EMD Millipore	Cat# sc-559389; lot# 2955375
Chorionic Gonadotropin	EMD Millipore	Cat#230734; lot# 2746020
XAV939	Sigma life science	Cat# X3004; lot# 0000034562

A-419259	Sigma life science	Cat# SML0446; lot# 0000033765
SB 431542	Sigma life science	Cat# sc- 204265A; lot# K2019
All trans-Retinoic Acid	Sigma life science	Cat# R2625
Geltrex™	Thermo Fisher Scientific	Cat# A1413201
Fibronectin	Thermo Fisher Scientific	Cat# 33016-015; lot# 1602739
Human FGF4 recombinant protein	Thermo Fisher Scientific	Cat# PHG0154
Human BMP4 recombinant protein	Thermo Fisher Scientific	Cat# PHC9534
Heparan sulfate sodium salt	Sigma life science	Cat# H7640
Human bFGF recombinant protein	Homemade	NA
Y-27632	Santa Cruz Biotechnology	Cat# sc- 281642A; lot# F2719
PMSG	Prospec	hor-272
hLIF	Homemade	NA
G418 disulfate salt	Sigma life science	Cat# A1720
Valproic acid	Tocris bioscience	Cat# 2815; lot# 1A/187243
Cell lines		
E14Tg2a		Chambers et al., 2007
TβC44Cre6		Chambers et al., 2007
TNGA		Chambers et al., 2007
ZHBTc4		Niwa et al., 2000
Oct4GiP		Ying et al., 2002
TCMC		Jana et al., 2019
TBCR	This Study	
ENOE	This Study	
OCT4$^{+/-}$	This Study	
EDiO	This Study	
TCMCOGFP	This Study	
HGFP	This Study	
ZHBTc4 NOE	This Study	
TCMC β-cat $^{-/-}$	This Study	
TCMCΔTEE	This Study	
TCMCΔIEE	This Study	
TCMCΔOBR	This Study	
TCMCΔONR	This Study	
TCMCΔONBR	This Study	
TCMCΔONBR HGFP	This Study	
ESTS	This Study	
ESTS HGFP	This Study	
Recombinant DNA		
pU6-(BbsI)-CBh-Cas9-T2A-mCherry	Addgene 64324	Weber et al., 2015

Mouse Oct4-GFP GOF18 transgenic reporter	Addgene 60527	Gafni et al., 2013
Oct4-IRES-eGFP-PGK-Neo	Addgene 48681	Yang et al 2013
pEFaNanog	This Study	
pMKiO	This Study	
pH2BGFP	This Study	
pU6-iRFP	This Study	
pU6-iRFP-β-cat $^{-/-}$	This Study	
pU6-iRFP- Oct4	This Study	
pU6-iRFP-ΔTEE	This Study	
pU6-iRFP-ΔIEE	This Study	
pU6-iRFP-ΔOBR	This Study	
pU6-iRFP-ΔNBR	This Study	
pU6-iRFP-ΔONBR	This Study	
Software and Algorithms		
ImageJ	ImageJ	RRID: SCR_003070
FlowJo	BD Bioscience	RRID: SCR_008520
Integrative genomics viewer	Broad Institute	RRID: SCR_011793
SDS	Applied Biosystems	RRID: SCR_015806
Image Lab	Bio-rad	RRID: SCR_014210
GraphPad Prism	GraphPad	RRID: SCR_002798
Zen Blue	Zeiss	RRID: SCR_013672
STAR	Dobin A et.al	RRID:SCR_004463
FastQC	Andrews, S	RRID:SCR_014583
RSEM	Li, B. et.al	RRID:SCR_013027
DESeq2	Love Ml et.al	RRID:SCR_015687
Cell Ranger	10x Genomics	RRID:SCR_017344
scater	Davis J McCarthy et.al	RRID:SCR_015954
Seurat	Hao and Hao et al.	RRID:SCR_016341
Scrublet	Wolock SL et.al	RRID:SCR_018098
HCLUST		RRID:SCR_009154
Other		
Lonza-4D Nucleofector	Lonza	N/A
BD LSR Fortessa	BD Bioscience	N/A
BD ARIA	BD Bioscience	N/A
MoFLo XDP	Beckman Coulter	N/A
Gallios Flow cytometer	Beckman Coulter	N/A
Chemidoc MP imaging system	Bio-rad	N/A
Zeiss Axio Observer	Zeiss	N/A
Zeiss Axio Zoom	Zeiss	N/A
Zeiss LSM 880	Zeiss	N/A
Olympus FV3000	Olympus	N/A
Leica SP8	Leica	N/A
Leica CM3000 UV Cryostat	Leica	N/A
TransferMan NK2	Eppendorf	N/A

10x Chromium System	10X Genomics	N/A
NovaSeq 6000 System	Illumina	N/A
Oligonucleotides		
Oligonucleotides used for qRTPCR		
Gene	Forward primer 5'->3'	Reverse primer 5'->3'
Oct4	GTGGAGGAAGCCGACAACAATGA	CAAGCTGATTGGCGATGTGAG
Nanog	TGGTCCCCACAGTTTGCCTAGTTC	CAGGTCTTCAGAGGAAGGGCGA
Klf4	GTGCAGCTTGCAGCAGTAAC	AGCGAGTTGGAAAGGATAAAGTC
Eomes	ACCAAAACACGGATATCACCCAGC	GGGACAATCTGATGGGATCTAGGGG
Gapdh	CAACGGCACAGTCAAGGCCGA	CCCTTCAAGTGGGCCCCGG
Cdx2	CCAGCTCACTTTTCCTCCTG	CAGCAGTCCCTAGGAAGCC
Elf5	TGGACCTAGCCACCACTTGTCT	TCACAGGCTGTCTGATGCTCAA
Gata3	TCCTTGCTACTCAGGTGATCGG	GCAGACACGGAGGAATAAAGGGG
Tcfap2c	CCACCGTGACCCCGATTGTG	GGCGATCCTCGCAATCCTCTTC
Hand1	CCTGGCTACCAGTTACATCGCC	TGCTGAGGCAACTCCCTTTTCC
Ctnnb1	ATGGAGCCGGACAGAAAAGC	CTTGCCACTCAGGGAAGGA
Ctsq	TGGAAAGAGTGGATGGGAAG	CAAGTGCACGTTTCCAGAGA
SynA	TACCCTGTCTGTGGACACCA	ACCAGAGGAGTTGAGGCAGA
SynB	TCGTCACCACCTTCTCACTG	TGGCTGTAGGCTCTCAGGTT
Tpbpa	TTCCTAGTCATCCTATGCCTGG	GGTCATTTTCGCTACTGTGAAGT
Tead4	GCACAGATCGTCTCGGCCACAG	GACTCAAAGCCTGGCAGAGGCAGC
Oligonucleotides used for sgRNA cloning		
Genomic region KO/KI	Guide 1	Guide 2
β-cat_KO	CACCGCAACACTCACTAGGCATGT	CACCGGCTGCCTCACACTAAGTTT
	AAACACATGCCTAGTGAGTGTTGC	AAACAAACTTAGTGTGAGGCAGCC
Cdx2_OBR_KO	CACCGAGTAAAGGGATCCAACCGGT	CACCGAGGGGTGTTTAAGGCCCCGC
	AAACACCGGTTGGATCCCTTTACTC	AAACGCGGGGCCTTAAACACCCCTC
Cdx2_NBR_KO	CACCGAGGGGTGTTTAAGGCCCCGC	CACCGCAGCCCCGCGCTATTTGTCA
	AAACGCGGGGCCTTAAACACCCCTC	AAACTGACAAATAGCGCGGGGCTGC

Cdx2_ONBR_KO	CACCGAGTAAAGGGATCCAACCGGT	CACCGCAGCCCCGCGCTATTTGTCA
	AAACACCGGTTGGATCCCTTTACTC	AAACTGACAAATAGCGCGGGGCTGC
Cdx2_TEE_KO	CACCGCCATAAATGACTTCCCCAAC	CACCGAACCAGACAGTCTAATTTG
	AAACGTTGGGGAAGTCATTTATGGC	AAACCAAATTAGACTGTCTGGTTC
Cdx2_IEE_KO	CACCGTCTGTCATAAAAGCGTCGTC	CACCGCTAGGAGGCGCGTGTGCTC
	AAACGACGACGCTTTTATGACAGAC	AAACGAGCACACGCGCCTCCTAGC
Cdx2_KI_last codon	CACCGAGACCACGGGAGGGGTCACT	
	AAACAGTGACCCCTCCCGTGGTCTC	
Oligonucleotides used for Genotyping		
Genomic Regions	Forward Primer Sequence 5'->3'	Reverse Primer Sequence 5'->3'
Cdx2 knockin	CCCTACTTGCACACCAACACTTTCT	GGCGATTCTCTTTTGCATGCTAGCAGGGCCGGGATTC
β Catenin	CTGGCAGCAGCAGTCTTACT	CCATGCCAGCACCCTTCTAC
Cdx2_O/N_BR	TGCTGCAGGTCCGAGGTTGTTCTGTCGTCTTCTGTGGAGTGG	TTTATCCCCCGAGGCAACTATCCT
Cdx2_intron1	CTAAGAGCAGCATCCGTTCTAGGG	GGCAACTATCCTGACCAAGTGACC
Cdx2_TEE	AGCCTAGGGTGAAGACTGTATCCC	TTTATGCCCAGCCCGGGACACACACACGGATGAATTGTCTGG
Cdx2_IEE	GAAGGCAACTTCCTCCATTAGCGA	GGAGCCCTTTTAGGTGTCTCCAAG

Cell Pedigree Chart

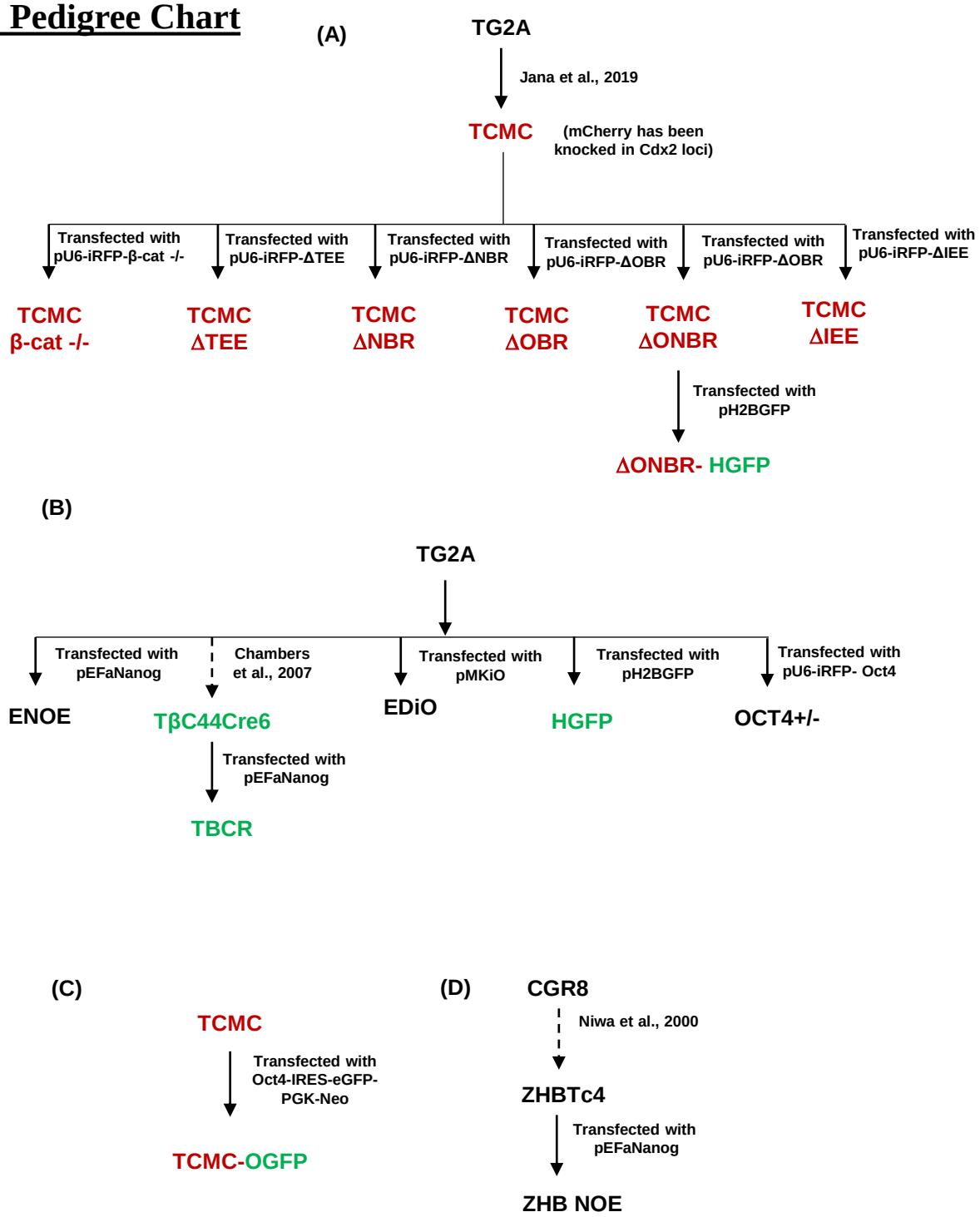

Figure : Information related to methods. A pedigree chart of cell lines used in this study (A)Flow chart illustrating the lineage and process of generation of TCMC and generation of knock out cells lines in TCMC background. (B) A flow chart Illustrating generation of engineered lines in E14Tg2a background . (C) A flow chart depicting derivation of knock-in cell line TCMC-OGFP in TCMC background. (D) A flow chart depicting generation of ZHB NOE from ZHBTc4.

Appendix 1

Generation of TCMC-OGFP

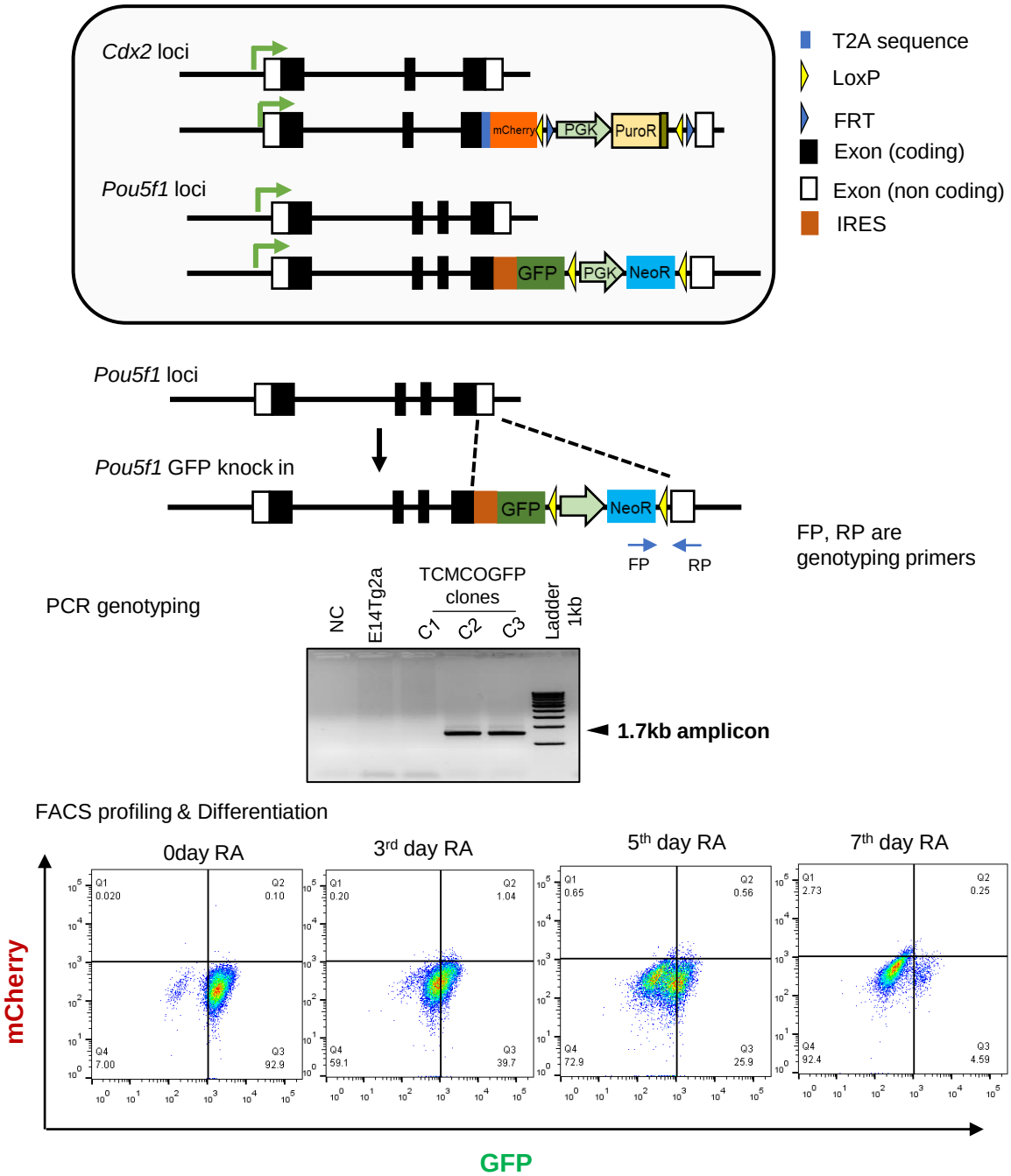

Generation of TCMC-OGFP (top) Schematic depiction of TCMC-OGFP cell line where one of the allele of *Oct4* has been knocked in with GFP and one of the allele of *Cdx2* has been knocked in with mCherry. The cell line has been derived from TCMC (middle) GFP knock in Oct4 loci has been confirmed by genotyping and sequencing. (bottom) FACS profile of GFP expression was used as a functional reporter for the knock-in GFP in *Oct4* loci with TCMC-OGFP cells grown in differentiating media with Retinoic acid (RA)

Appendix 2

Generation of TCMC-β-Catenin-/-

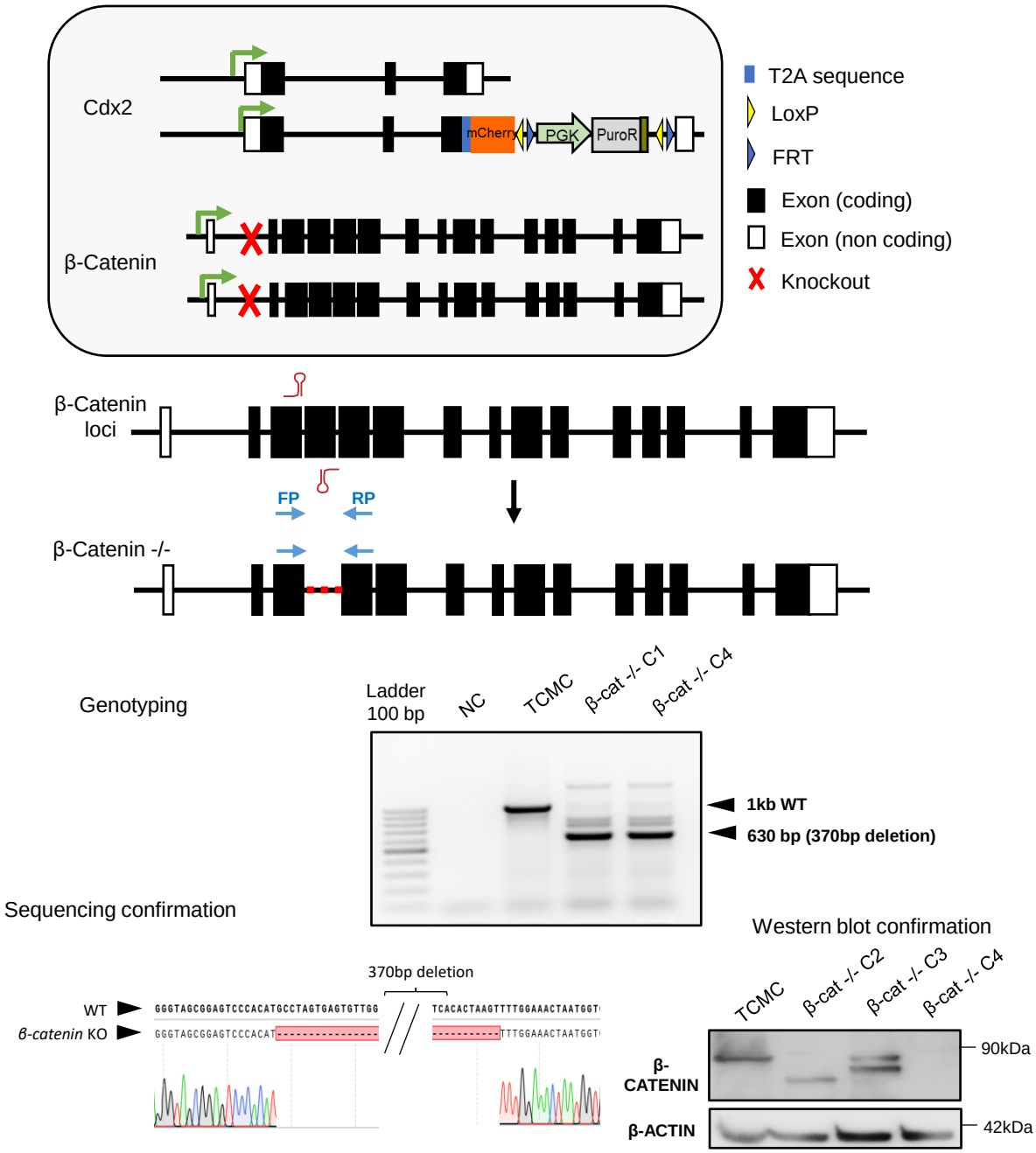

Generation of TCMC-β-Catenin-/- ES cell line(top) Schematic depiction of TCMC-β-catenin $^{-/-}$ ES cell line. The cell line has been derived from TCMC (middle) β-catenin $^{-/-}$ has been confirmed by genotyping encompassing the deletion site. and sequencing. (bottom) Western blotting for different clones were confirmed by checking β- CATENIN.

Appendix 3

Generation of TCMCΔOBR

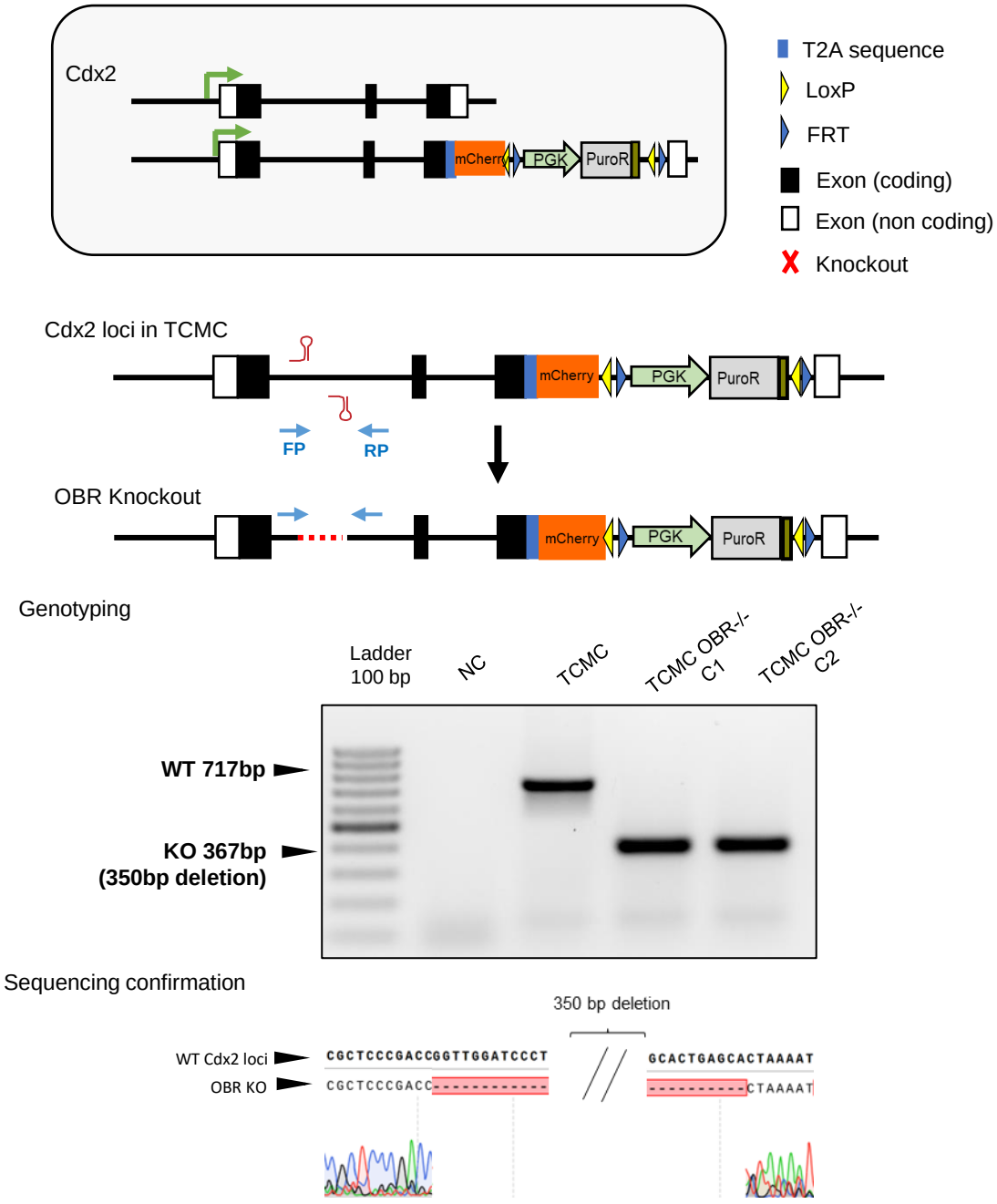

Generation of TCMCΔOBR (top) Schematic depiction of TCMCΔOBR The cell line has been derived from TCMC (middle) ΔOBR has been confirmed by genotyping different clones encompassing the deletion site. (bottom) Sequencing confirmation of the genotyped PCR product.

Appendix 4

Generation of TCMCΔNBR

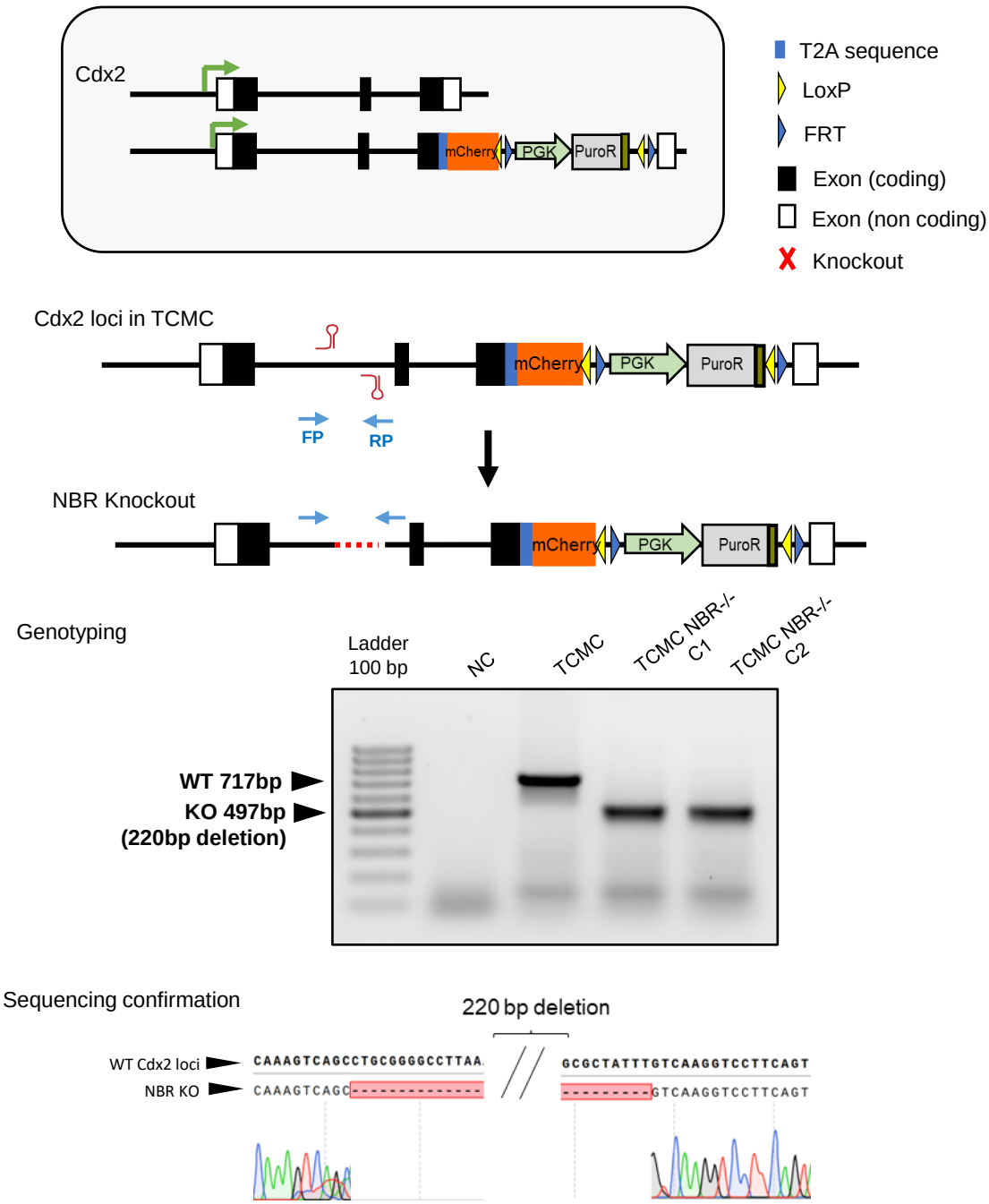

Generation of TCMCΔNBR (top) Schematic depiction of TCMCΔNBR The cell line has been derived from TCMC (middle) ΔNBR has been confirmed by genotyping different clones encompassing the deletion site. (bottom) Sequencing confirmation of the genotyped PCR product.

Appendix 5

Generation of TCMCΔONBR

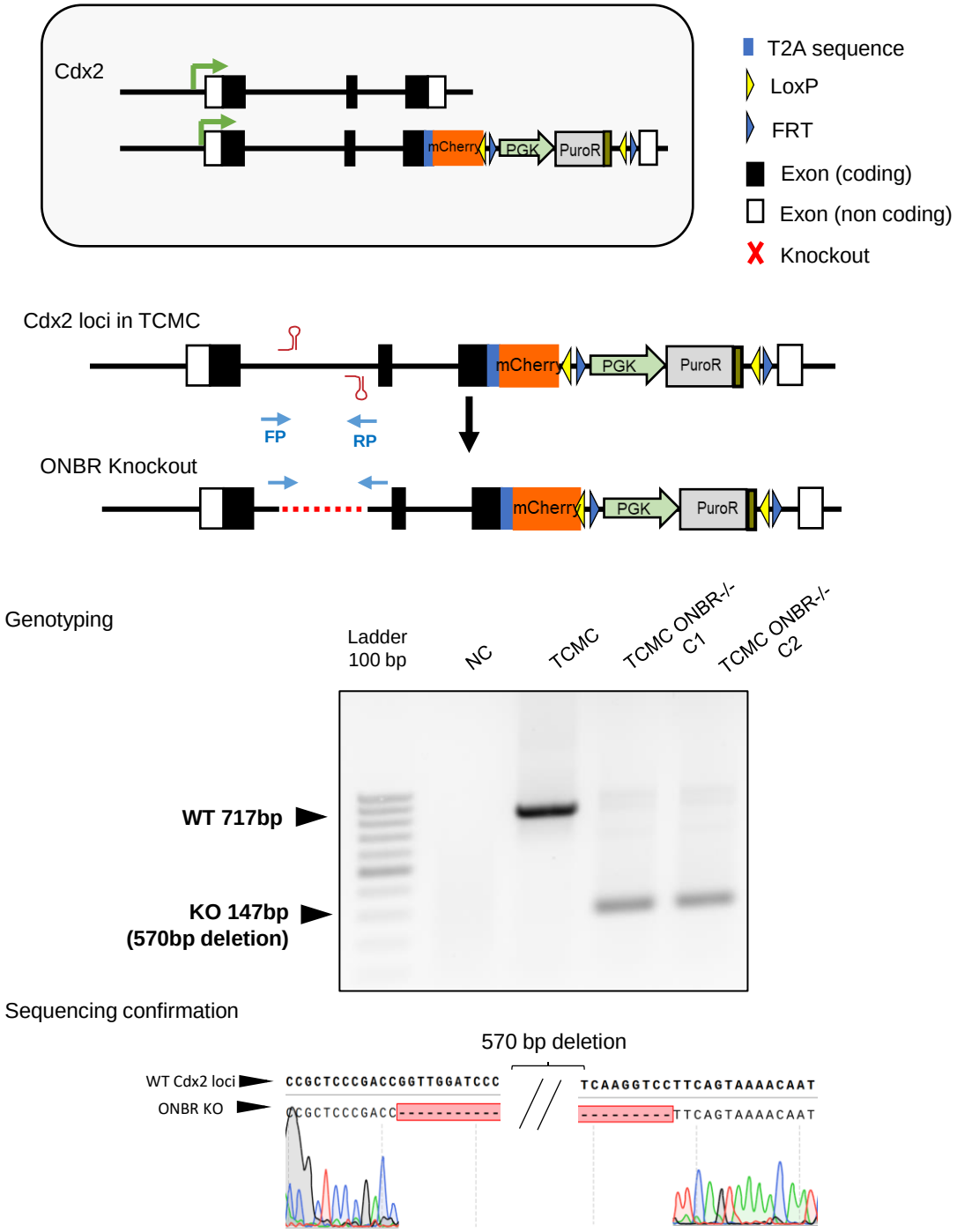

Generation of TCMCΔONBE (top) Schematic depiction of TCMCΔONBR The cell line has been derived from TCMC (middle) ΔONBR has been confirmed by genotyping different clones encompassing the deletion site. (bottom) Sequencing confirmation of the genotyped PCR product.

Appendix 6

Generation of TCMCΔTEE

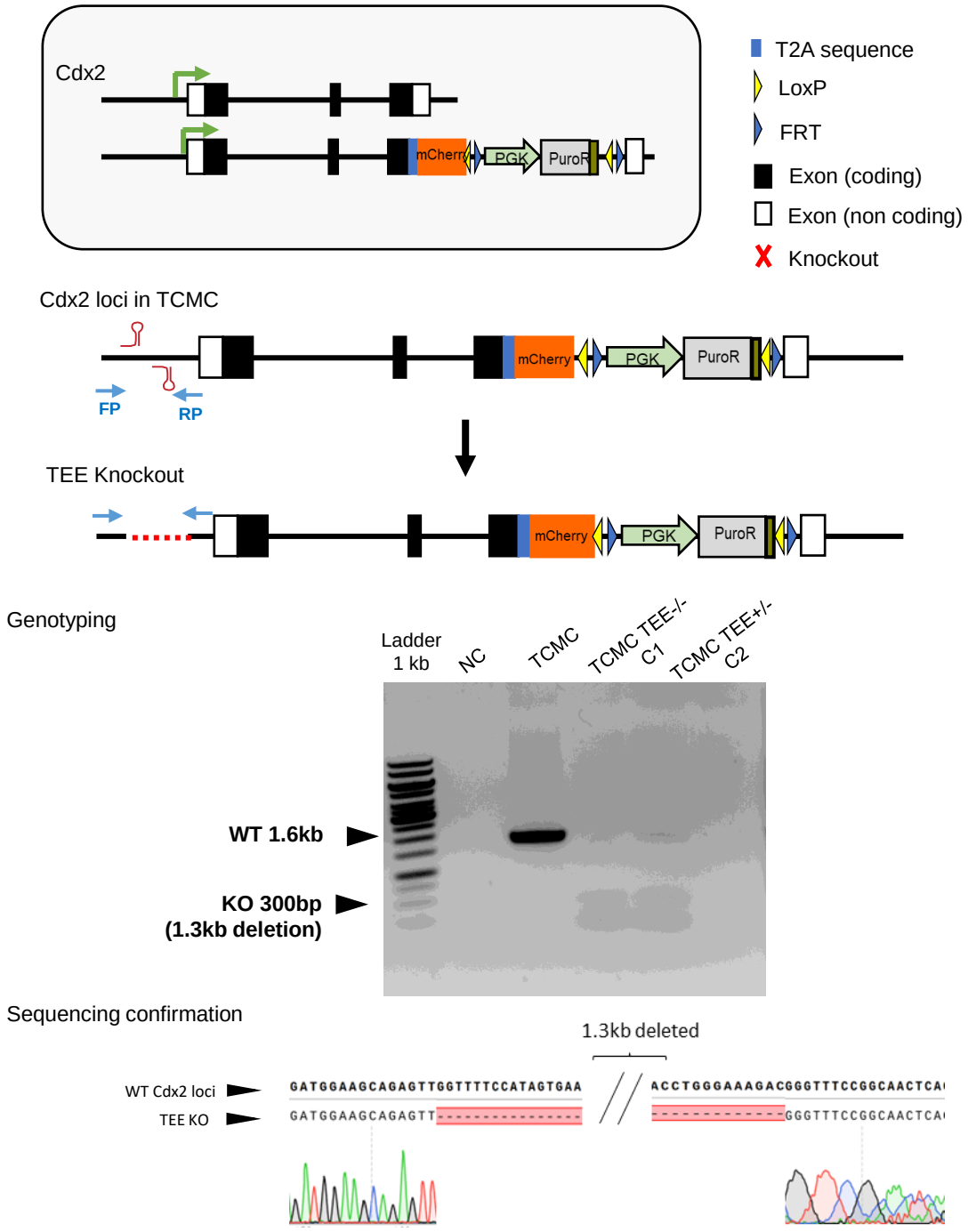

Generation of TCMCΔIEE (top) Schematic depiction of TCMCΔTEE The cell line has been derived from TCMC (middle) ΔTEE has been confirmed by genotyping different clones encompassing the deletion site. (bottom) Sequencing confirmation of the genotyped PCR product.

Appendix 7

Generation of TCMCΔIEE

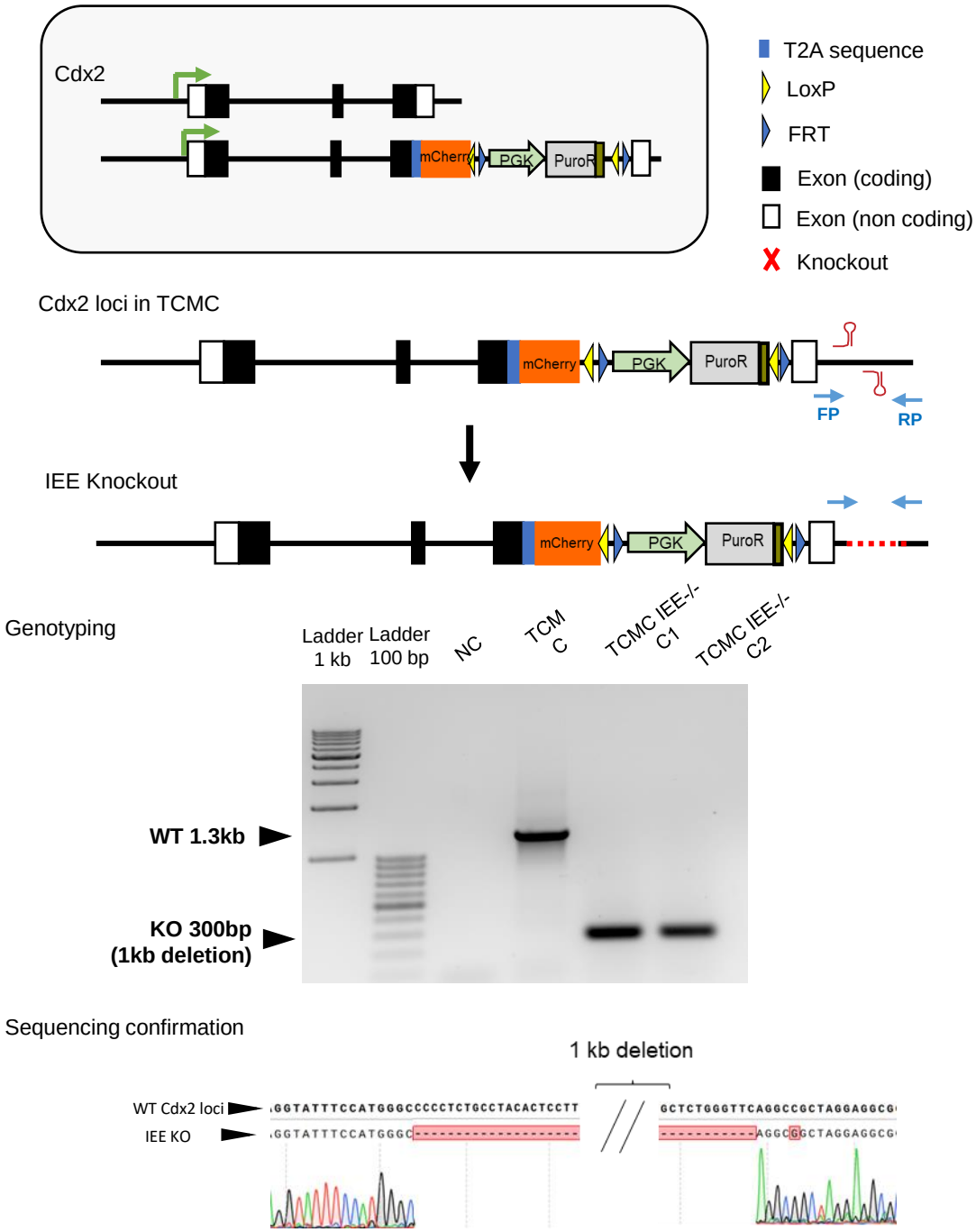

Generation of TCMCΔIEE (top) Schematic depiction of TCMCΔIEE The cell line has been derived from TCMC (middle) ΔIEE has been confirmed by genotyping different clones encompassing the deletion site. (bottom) Sequencing confirmation of the genotyped PCR product.